

Augmented quantization: a general approach to mixture models

Charlie Sire

IRSN, BRGM, Mines Saint-Etienne, Univ. Clermont Auvergne, CNRS, UMR 6158 LIMOS
and

Didier Rullière

Mines Saint-Etienne, Univ. Clermont Auvergne, CNRS, UMR 6158 LIMOS
and

Jérémy Rohmer

BRGM

and

Rodolphe Le Riche

CNRS, Mines Saint-Etienne, Univ. Clermont Auvergne, UMR 6158 LIMOS
and

Lucie Pheulpin

IRSN

and

Yann Richet

IRSN

Abstract

The investigation of mixture models is a key to understand and visualize the distribution of multivariate data. Most mixture models approaches are based on likelihoods, and are not adapted to distribution with finite support or without a well-defined density function. This study proposes the Augmented Quantization method, which is a reformulation of the classical quantization problem but which uses the p -Wasserstein distance. This metric can be computed in very general distribution spaces, in particular with varying supports. The clustering interpretation of quantization is revisited in a more general framework. The performance of Augmented Quantization is first demonstrated through analytical toy problems. Subsequently, it is applied to a practical case study involving river flooding, wherein mixtures of Dirac and Uniform distributions are built in the input space, enabling the identification of the most influential variables.

Contents

1	Introduction	3
2	Augmented quantization	4
2.1	Problem formulation	4
2.2	From K-means to Augmented Quantization	5
3	Definition and properties of quantization errors	7
3.1	Quantization and global errors	7
3.2	Clustering error	8
4	Algorithm steps	9
4.1	Finding clusters from representatives	9
4.2	Perturb clusters	10
4.3	Finding representatives from clusters	13
4.4	Implementation aspects	13
5	Toy problems with homogeneous mixtures	13
5.1	1D uniform example	13
5.2	A mixture of Dirac example	17
5.3	A Gaussian mixture example	19
6	An hybrid mixture test case	21
7	Application to river flooding	22
8	Summary and perspectives	25
A	Expectation-Maximization with uniform mixtures	29
A.1	Lower and upper bounds	29
A.2	Details of the Expectation-Maximization approach	29
B	Removing clusters perturbation step	30
C	Proof of Proposition 1	30
D	Proof of clustering consistency (Proposition 3)	32
D.1	Convergence in law of the mixture samples designated by the clustering	33
D.1.1	Convergence in law of $a_N(X_k)$	33
D.1.2	Convergence in law of $a_N(X_k) \mid J_{I_N(X_k)} = j$	34
D.2	Wasserstein convergence to the representatives	36
D.2.1	Wasserstein convergence of $a_N(\tilde{X}_{k,N}^{(j)})$	36
D.2.2	Wasserstein convergence of $(a_N(\tilde{X}_{k,N}^{(j)}))_{k=1}^n$	36
D.2.3	Wasserstein convergence of $C_j^*(R, J, n, N)$ to R_j	37
D.3	Convergence of the expected quantization error	37

E	Merging the split clusters	38
F	An implementation of the Augmented Quantization algorithm	39
G	Evolution of the quantization error	40
H	Flooding prototype maps	41

1 Introduction

Quantization methods classically provide discrete representations of continuous distributions [8]. Quantization is a key component of digitalization in signal processing [16] and, more generally, it can be employed as a clustering technique to approximate continuous random variables with a Dirac mixture [19]. This representation is useful when describing continuous phenomena with a finite number of prototype elements. Discrete approximations to random variables are classically obtained by minimizing a Maximum Mean Discrepancy [25] or as centroids of Voronoi cells in the K-means clustering [10].

However, when approximating a random variable, it may be desirable to come up with a representation that is more complex than a discrete distribution. Mixture models are relevant in this case. They aim to identify subpopulations in a sample that arise from a common distribution but with different parameters [1]. Gaussian mixture models are probably the most popular and highlight normally distributed subgroups. Mixture models, which can be seen as clustering methods, expand conventional quantization by allowing the use of any distribution in place of the Dirac measure. The mixture is learned with the Expectation-Maximization (EM) algorithm [5], which performs a probabilistic assignment of each point to a cluster by the computation of likelihoods, followed by the estimation of the cluster parameters by likelihood maximization. In certain applications, it is necessary to study specific distributions mixes. For example, in the flooding case study (cf. Section 7) where the objective is to gain insights into the influence of variables in relation to specific flood spatial patterns, we investigate subdistributions that consist either of a Dirac measure at a specific value or a uniform distribution with its support. Here, larger supports denote less influential variables.

Learning very general distributions is not easy. Distributions such as the uniform or the Dirac measure overlook points out of their supports and processing them through likelihoods and such direct functionals of their density will fail. Appendix A illustrates this problem with uniform distributions whose supports include all the points, even the obvious outliers. Density is not even defined when it comes to Dirac mixtures or to distributions with singular components. One possible remedy is to work with zero-inflated beta distributions [2], but they remain less general and harder to interpret than the well-known uniform, Dirac, or Gaussian distributions.

Thus, one objective of this article is to establish a framework for learning

mixtures of general distributions. Our approach is based on computing the p -Wasserstein distance between two probability measures, μ and ν , on a space \mathcal{X} , without strong restrictions on them [26]. In particular, the p -Wasserstein distance is defined between measures that do not have the same support or when one is discrete and the other continuous. The p -Wasserstein distance is defined as follows:

$$\mathcal{W}(\mu, \nu) = \inf_{\pi \in \Pi(\mu, \nu)} \left(\int_{\mathcal{X} \times \mathcal{X}} \|x - x'\|^p \pi(dx, dx') \right)^{\frac{1}{p}},$$

where $\Pi(\mu, \nu)$ is the set of all the joint probability measures on $\mathcal{X} \times \mathcal{X}$ whose marginals are μ and ν on the first and second factors, respectively. This metric represents the optimal transport cost between the two measures and appears highly relevant in our context of approximation of a set of points by a general mixture.

However, finding the best mixture of ℓ different distributions (for a given $\ell \in \mathbb{N}$) is not straightforward, as calculating the weights and parameters of the distributions implies minimizing p -Wasserstein distances which are non-convex optimization problems [12]. In addition, learning mixtures of distributions generates problems with many variables. For instance, a mixture of 4 Dirac measures in 4 dimensions is described by 20 variables.

Clustering approaches like K-means are popular in such high-dimensional situations. They reduce the size of the optimization problem by decomposing it cluster by cluster. Clustering also facilitates the interpretation of the results. Our method, that we call Augmented Quantization (AQ), is based on the classical K-means, generalized to handle various types of distributions using the p -Wasserstein distance.

The paper is structured as follows. The problem is formulated and a path towards Augmented Quantization is sketched in Section 2. Elements of analysis of Augmented Quantization are given in Section 3 followed, in Section 4, by a description of the implementation steps of the algorithm. In Section 5, the method is applied to several toy problems and compared to existing approaches, while in Section 7, it is applied to a study of real floodings. Finally, Section 8 summarizes the main results and proposes extensions to the method.

2 Augmented quantization

2.1 Problem formulation

The objective of the study conducted here is to build a very general mixture model that approximates the (unknown) underlying distribution of a (known) sample $(x_i)_{i=1}^n \in \mathcal{X}^n$ with $\mathcal{X} \subset \mathbb{R}^m$.

The components of the mixture, called representatives, will be seen as probability measures on \mathcal{X} . They belong to a given family of probability measures

which is not necessarily parametric. More precisely, we consider $\ell \in \mathbb{N}^*$ representatives named through their tag taken in $\mathcal{J} = \{1, \dots, \ell\}$. Let \mathcal{R} be a family of probability measures, the objective is approximate the distribution of $(x_i)_{i=1}^n$ by the mixture R_J such that

- $R_J = \sum_{j \in \mathcal{J}} \mathbb{P}(J = j) R_j$,
- $R_j \in \mathcal{R}$, $j \in \mathcal{J}$,
- J a discrete random variable independent of (R_1, \dots, R_ℓ) with weights $p_j = P(J = j)$, $j \in \mathcal{J}$.

It is important to note that this representation is not necessarily unique, the identifiability of the problem depends on the family \mathcal{R} [27]. For instance, a mixture of the measures associated to $\mathcal{U}(0.5, 1)$ and $\mathcal{U}(0, 1)$ with weights 0.5 on one hand, and a mixture of the measures associated to $\mathcal{U}(0, 0.5)$ and $\mathcal{U}(0.5, 1)$ with respective weights 0.25 and 0.75 on the other hand, are identical.

Augmented quantization, as the name indicates, generalizes the traditional quantization method and the accompanying K-means clustering. Let us first recall the basics of K-means. In K-means, the representatives are Dirac measures located at γ , $\mathcal{R} = \{\delta_\gamma, \gamma \in \mathcal{X}\}$. For a given set of representatives $\mathbf{R} = (R_1, \dots, R_\ell) = (\delta_{\gamma_1}, \dots, \delta_{\gamma_\ell}) \in \mathcal{R}^\ell$, the associated clusters are $\mathbf{C} = (C_1, \dots, C_\ell)$ with $C_j = \{x \in (x_i)_{i=1}^n : j = \arg \min_{i \in \mathcal{J}} \|x - \gamma_i\|\}$, $j \in \mathcal{J}$. The objective is to minimize the *quantization error*,

$$\mathcal{E}_p(\gamma_1, \dots, \gamma_\ell) := \left(\frac{1}{n} \sum_{i=1}^n \|x_i - \arg \min_{\gamma \in \Gamma_\ell} \|x_i - \gamma\|\|^p \right)^{\frac{1}{p}}. \quad (1)$$

We now generalize the quantization error by replacing the Euclidean distance with a p -Wasserstein metric which, it turns, allows to rewrite the quantization error for any representatives \mathbf{R} and associated clusters \mathbf{C} :

$$\mathcal{E}_p(\mathbf{C}, \mathbf{R}) := \left(\sum_{j=1}^{\ell} \frac{\text{card}(C_j)}{n} \mathcal{W}_p(C_j, R_j)^p \right)^{\frac{1}{p}}, \quad (2)$$

where $\mathcal{W}_p(C_j, R_j)$ is the p -Wasserstein distance [20] between the empirical probability measure associated to C_j and the measure R_j .

The traditional quantization error (1) is recovered from the general error 2 by limiting the representatives to Dirac measures and defining the clusters as nearest neighbors to the Dirac locations γ_i , $i = 1, \dots, \ell$. The general clusters C_j , $j = 1, \dots, \ell$ of Equation 2 form a partition of the samples $(x_i)_{i=1}^n$. We will soon see how to define them.

2.2 From K-means to Augmented Quantization

Lloyd's algorithm is one of the most popular implementation of K-means quantization [6]. The method can be written as follows:

Algorithm 1 Lloyd's algorithm

Input: $(\gamma_1, \dots, \gamma_\ell) \in \mathcal{X}^\ell$, sample $(x_i)_{i=1}^n$

while stopping criterion not met **do**

FindC : update the clusters,

$$\forall j \in \mathcal{J}, C_j = \{x \in (x_i)_{i=1}^n : j = \arg \min_{j' \in \mathcal{J}} \|x - \gamma_{j'}\|\}$$

FindR : update the representatives,

$$\forall j \in \mathcal{J}, \gamma_j = \frac{1}{\text{card}(C_j)} \sum_{x \in C_j} x, \quad R_j = \delta_{\gamma_j}$$

end while

Output:

- the membership discrete random variable J with $\mathbb{P}(J = j) = \frac{\text{card}(C_j)}{n}$, $j \in \mathcal{J}$
 - the mixture $R_J = \sum_{j \in \mathcal{J}} \mathbb{P}(J = j) \delta_{\gamma_j}$
-

Algorithm 1 is not the standard description of Lloyd's algorithm but an interpretation paving the way towards augmented quantization and the estimation of mixture distributions: the centroids $(\gamma_1, \dots, \gamma_\ell)$ are seen as representatives (R_1, \dots, R_ℓ) through the Dirac measures δ_γ ; the produced Voronoi cells are translated into a mixture distribution.

At each iteration, new clusters $\mathbf{C} = (C_1, \dots, C_\ell)$ are determined from the previously updated representatives (centroids in this case), and then new representatives $\mathbf{R} = (R_1, \dots, R_\ell)$ are computed from the new clusters. These operations reduces the quantization error. We refer to these two steps as *FindC* and *FindR*. The stopping criterion is typically related to a very slight difference between the calculated representatives and those from the previous iteration.

The usual quantization is augmented by allowing representatives that belong to a predefined set of probability measures \mathcal{R} . In Augmented Quantization, \mathcal{R} can still contain Dirac measures but it will typically include other measures. Each iteration alternates between \mathbf{C} during *FindC* and the mixture defined by (\mathbf{R}, J) during *FindR*. *FindC* is now a function which partitions $(x_i)_{i=1}^n$ into clusters based on a set of the representatives and the random membership variable J . *FindR* is a function which generates a set of representatives from a partition of $(x_i)_{i=1}^n$. Algorithm 2 is the skeleton of the Augmented Quantization algorithm.

Lloyd's algorithm can be seen as descent algorithm applied to the minimization of the quantization error (Equation (1)). It converges to a stationary point

which may not even be a local optimum [21]. Although Lloyd’s algorithm converges generally to stationary points that have a satisfactory quantization error, Appendix B illustrates that its generalization to continuous distributions does not lead to a quantization error sufficiently close to the global optimum. To overcome this limitation, an additional mechanism for exploring the space of mixture parameters is needed. To this aim, we propose a perturbation of the clusters called *Perturb()*, which takes place between *FindC* and *FindR*.

Algorithm 2 Augmented Quantization algorithm

Input: $\mathbf{R} = (R_1, \dots, R_\ell) \in \mathcal{R}^\ell$, samples $(x_i)_{i=1}^n$

$J \in \mathcal{J}$ r.v. with $\mathbb{P}(J = j) = \frac{1}{\ell}$
 $(R^*, C^*, \mathcal{E}^*) \leftarrow (\emptyset, \emptyset, +\infty)$

while stopping criterion not met **do**

 Update clusters: $\mathbf{C} \leftarrow \text{FindC}(\mathbf{R}, J)$

 Perturb clusters: $\mathbf{C} \leftarrow \text{Perturb}(\mathbf{C})$

 Update mixture: $\mathbf{R} \leftarrow \text{FindR}(\mathbf{C})$, J r.v. with $\mathbb{P}(J = j) = \frac{\text{card}(C_j)}{n}$, $j \in \mathcal{J}$

 Update the best configuration:

if $\mathcal{E}_p(\mathbf{C}, \mathbf{R}) < \mathcal{E}^*$ **then** $\mathcal{E}^* \leftarrow \mathcal{E}$, $C^* \leftarrow C$, $R^* \leftarrow R$, $J^* \leftarrow J$

end while

Output:

- the membership discrete random variable J^* with $\mathbb{P}(J^* = j) = \frac{\text{card}(C_j^*)}{n}$, $j \in \mathcal{J}$
 - the mixture $R_{j^*}^*$.
-

3 Definition and properties of quantization errors

Before describing in details the *FindC*, *Perturb* and *FindR* steps, some theoretical elements are provided that will be useful to explain our implementation choices.

3.1 Quantization and global errors

Let $\mathbf{R} = (R_1, \dots, R_\ell)$ be ℓ probability measures and $\mathbf{C} = (C_1, \dots, C_\ell)$ be ℓ disjoint clusters of points in $\mathcal{X} \subset \mathbb{R}^d$. Let us denote $n_j = \text{card}(C_j)$ for $j \in \mathcal{J}$, and $n = \sum_{j=1}^n n_j$.

The *quantization error* between \mathbf{C} and \mathbf{R} is defined by

$$\mathcal{E}_p(\mathbf{C}, \mathbf{R}) := \left(\sum_j^\ell \frac{n_j}{n} \mathcal{W}_p(C_j, R_j)^p \right)^{1/p}. \quad (3)$$

It should not be mistaken with the *global error* between \mathbf{C} and \mathbf{R} , which is defined by

$$\epsilon_p(\mathbf{C}, \mathbf{R}) := \mathcal{W}_p \left(\bigcup_{j=1}^\ell C_j, R_J \right), \quad (4)$$

where $J \in \mathcal{J}$ is a random variable such that $\mathbb{P}(J = j) = \frac{n_j}{n}$. The quantization error aggregates the local errors between the clusters and the representatives, while the global error characterizes the overall mixture.

The quantization error is a natural measure of clustering performance and clustering is a way to decompose the minimization of the global error. Such a decomposition is justified by Proposition 1, which shows that a low quantization error guarantees a low global error.

Proposition 1 (Global and quantization errors).

The global error between a clustering \mathbf{C} and a set of representatives \mathbf{R} is lower than the quantization error between them:

$$\epsilon_p(\mathbf{C}, \mathbf{R}) = \mathcal{W}_p \left(\bigcup_{j=1}^\ell C_j, R_J \right) \leq \left(\sum_j^\ell \frac{n_j}{n} \mathcal{W}_p(C_j, R_j)^p \right)^{1/p} = \mathcal{E}_p(\mathbf{C}, \mathbf{R}).$$

The proof is provided in Appendix C.

3.2 Clustering error

For a given clustering $\mathbf{C} = (C_1, \dots, C_\ell)$, the optimal representatives can be calculated individually for each cluster. This optimization allows to introduce the notion of quantization error of a clustering.

Proposition 2 (Quantization error of a clustering). *Let $\mathbf{C} = (C_1, \dots, C_\ell)$ be ℓ clusters of points in \mathcal{X} and the associated optimal representatives*

$$\mathbf{R}^*(\mathbf{C}) := \arg \min_{\mathbf{R} \in \mathcal{R}^\ell} \mathcal{E}_p(\mathbf{C}, \mathbf{R}).$$

Then:

- (i) *The optimal representatives can be optimized independently for each cluster,*

$$\mathbf{R}^*(\mathbf{C}) = (R_1^*(C_1), \dots, R_\ell^*(C_\ell)) \text{ where } R_j^*(C_j) := \arg \min_{r \in \mathcal{R}} \mathcal{W}_p(C_j, r), j \in \mathcal{J}.$$

This results trivially from the fact that \mathcal{E}_p is a monotonic transformation of a sum of independent components.

(ii) The local error of a cluster C_j is defined as the p -Wasserstein distance between C and its optimal representative $R_j^*(C_j)$,

$$w_p(C_j) := \mathcal{W}_p(C_j, R_j^*(C_j)) = \min_{r \in \mathcal{R}} \mathcal{W}_p(C_j, r) .$$

(iii) The quantization error of a clustering \mathbf{C} is the quantization error between \mathbf{C} and $\mathbf{R}^*(\mathbf{C})$, its associated optimal representatives,

$$\mathcal{E}_p(\mathbf{C}) := \mathcal{E}_p(\mathbf{C}, \mathbf{R}^*(\mathbf{C})) = \min_{\mathbf{R} \in \mathcal{R}^\ell} \mathcal{E}_p(\mathbf{C}, \mathbf{R}) .$$

(iv) The global error associated to a clustering \mathbf{C} is lower than its quantization error,

$$\epsilon_p(\mathbf{C}) \leq \mathcal{E}_p(\mathbf{C})$$

with $\epsilon_p(\mathbf{C}) = \epsilon_p(\mathbf{C}, \mathbf{R}^*(\mathbf{C})) = \mathcal{W}_p(\bigcup_{j=1}^{\ell} C_j, R_j^*(C_j))$ and $\mathbb{P}(J = j) = \frac{n_j}{n}$, $j \in \mathcal{J}$. This follows directly from Proposition 1.

The above clustering error is based on a p -Wasserstein distance minimization in the space of probability measures \mathcal{R} . This problem is further addressed in Section 4.3 when seeking representatives from given clusters.

4 Algorithm steps

The steps of the Augmented Quantization algorithm can now be presented in details. We will explain how they contribute to reducing the quantization error which was discussed in Section 3.

4.1 Finding clusters from representatives

At this step, a mixture distribution R_J is given through its ℓ representatives $\mathbf{R} = (R_1, \dots, R_\ell)$ and the associated membership random variable J such that $P(J = j) = p_j$, $j = 1, \dots, \ell$. Clustering is performed by, first, creating N samples from the mixture distribution: the membership variable j is sampled from J , and each point is drawn from R_j . Second, the data points are assigned to the cluster to which belongs the closest of the N samples. Before returning to the algorithm, we provide a theoretical justification for it.

Let $(X_i)_{i=1}^n \in \mathcal{X}^n$ be a random sample of the above R_J mixture distribution. $(J_i)_{i=1}^N$ are i.i.d. samples with the same distribution as J , and $(Y_i)_{i=1}^N$ i.i.d. samples with $Y_i \sim R_{J_i}$, $i = 1, \dots, N$. We define the following clustering,

$$\begin{aligned} \mathbf{C}^*(R, J, n, N) &:= \left(C_1^*(R, J, n, N), \dots, C_\ell^*(R, J, n, N) \right) , \\ \text{with } C_j^*(R, J, n, N) &:= \{X_k \text{ s.t. } J_{I_N(X_k)} = j, 1 \leq k \leq n\} , \\ \text{and } I_N(x) &:= \arg \min_{i=1, \dots, N} \|x - Y_i\| . \end{aligned}$$

We work with general distributions that are combinations of continuous and discrete distributions,

$$\mathcal{R}_s := \{\beta_c R_c + \beta_{\text{disc}} R_{\text{disc}}, R_c \in \mathcal{R}_c, R_{\text{disc}} \in \mathcal{R}_{\text{disc}}, \beta_c + \beta_{\text{disc}} = 1\}.$$

\mathcal{R}_c and $\mathcal{R}_{\text{disc}}$ are the set of measures associated to almost everywhere continuous distributions with finite support, and, the set of measures associated to discrete distributions with finite support, respectively.

In the family of probability measures R_s , the above clustering is asymptotically consistent: the *quantization error* associated to this clustering is expected to tend to zero as n and N increase.

Proposition 3. *If $R_j \in \mathcal{R}_s$ for $j \in \mathcal{J}$ and $X_i \sim R_{J_i^X}$, $i = 1, \dots, n$ with $(J_i^X)_{i=1}^n$ i.i.d. sample with same distribution as J , then*

$$\lim_{n, N \rightarrow +\infty} \mathbb{E} (\mathcal{W}_p(C_j^*(R, J, n, N), R_j)) = 0, \quad j \in \mathcal{J}.$$

As a consequence,

$$\lim_{n, N \rightarrow +\infty} \mathbb{E} (\mathcal{E}_p(\mathbf{C}^*(R, J, n, N))) = 0.$$

The proof along with further details about \mathcal{R}_s are given in Appendix D.

The objective of the *FindC* procedure is to associate a partition of a sample $(x_i)_{i=1}^n$ to the representatives \mathbf{R} with probabilistic weights defined by the random variable J . It is described in Algorithm 3.

Algorithm 3 *FindC*

Input: Sample $(x_i)_{i=1}^n$, $\mathbf{R} = (R_1, \dots, R_\ell)$, N , J r.v. $\in \mathcal{J}$

$C_j = \emptyset$, $j \in \mathcal{J}$
 $(j_i)_{i=1}^N$ N independent realizations of J
 $(y_i)_{i=1}^N$ N independent realizations, y_i sampled with associated measure R_{j_i}
for $x \in (x_i)_{i=1}^n$ **do**
 $I(x) \leftarrow \arg \min_{i=1, \dots, N} \|x - y_i\|$
 $C_{j_{I(x)}} \leftarrow C_{j_{I(x)}} \cup x$
end for

Output: Partition $\mathbf{C} = (C_1, \dots, C_\ell)$

The *FindC* algorithm is consistent in the sense of the above Proposition 3.

4.2 Perturb clusters

Once clusters are associated to representatives, the *Perturb* step is required to explore the space of partitions of $(x_i)_{i=1}^n$. Appendix B illustrates why such a step is important through the example of a mixture of two uniforms that,

without perturbation, cannot be identified from a given, seemingly reasonable, starting clustering. Thus, a relevant cluster perturbation should be sufficiently exploratory. To increase convergence speed, we make it greedy by imposing a systematic decrease in quantization error.

Proposition 4 (Greedy cluster perturbation).

Let $\mathbf{C} = (C_1, \dots, C_\ell)$ be a clustering, and $G(\mathbf{C})$ a set of perturbations of this clustering such that $\mathbf{C} \subset G(\mathbf{C})$.

The greedy perturbation, $\text{Perturb}()$, is a function that yields a new clustering $\mathbf{C}^* = \text{Perturb}(\mathbf{C})$ through $\mathbf{C}^* := \arg \min_{\mathbf{C}' \in G(\mathbf{C})} \mathcal{E}_p(\mathbf{C}')$.

Trivially, $\mathcal{E}_p(\mathbf{C}^*) \leq \mathcal{E}_p(\mathbf{C})$.

The quantization error decrease comes from the inclusion of the current clustering in the set of perturbations. Here, we choose to perturb the clusters through the identification of the points contributing the most to the quantization error.

The need for a perturbation has also been described in classical K-means methods where it takes the form of a tuning of the initial centroids when restarting the algorithm [3].

Our cluster perturbation consists in, first, identifying the elements to move which defines the *split* phase and, second, reassigning them to other clusters in what is the *merge* phase.

split phase

The clusters with the ℓ_{bin} highest local errors w_p will be split. Their indices make the $\text{indexes}_{\text{bin}}$ list. During the *split* phase, for each cluster $C_j, j \in \text{indexes}_{\text{bin}}$, a proportion of p_{bin} points are sequentially removed and put in a sister “bin” cluster. A point x^* is removed from the cluster if the clustering composed of the cluster after point removal and the bin cluster has the lowest error.

The values of ℓ_{bin} and p_{bin} determine the magnitude of the perturbations. Their values will be discussed after the *merge* procedure is presented. Algorithm 4 sums up the *split* procedure.

Algorithm 4 *split* procedure

Input: a sample $(x_i)_{i=1}^n$, a partition $\mathbf{C} = (C_1, \dots, C_\ell)$, $p_{\text{bin}} \in [0, 1]$, $\text{indexes}_{\text{bin}} = \{j_1, \dots, j_{\ell_{\text{bin}}}\}$

```
for  $j \in \text{indexes}_{\text{bin}}$  do
   $C_j^{\text{bin}} \leftarrow \emptyset$ 
   $n_{\text{bin}} \leftarrow p_{\text{bin}} \text{card}(C_j)$ 
  while  $\text{card}(C_j^{\text{bin}}) < n_{\text{bin}}$  do
     $x^* \leftarrow \arg \min_{x \in C_j} \mathcal{E}_p(\mathbf{C}_j^{\text{split}}(x))$    where    $\mathbf{C}_j^{\text{split}}(x) = (C_j \setminus x, C_j^{\text{bin}} \cup x)$ 
     $C_j^{\text{bin}} \leftarrow C_j^{\text{bin}} \cup x^*$ 
     $C_j \leftarrow C_j \setminus x^*$ 
  end while
end for
```

Output: a partition $\hat{\mathbf{C}} = \text{split}(\mathbf{C}) = (C_1, \dots, C_\ell, C_{j_1}^{\text{bin}}, \dots, C_{j_{\ell_{\text{bin}}}}^{\text{bin}})$

merge phase

The *merge* procedure goes back to ℓ clusters by combining some of the $\ell + \ell_{\text{bin}}$ clusters together. The approach here simply consists in testing all the possible mergings to go from $\ell + \ell_{\text{bin}}$ to ℓ groups, and in keeping the one with the lowest quantization error. The full algorithm is provided in Appendix E.

If \mathcal{P} is the set of all partitions of $1, \dots, \ell + \ell_{\text{bin}}$ into ℓ groups, the number of possible mergings, which is the cardinal of \mathcal{P} , is equal to the Stirling number of the second kind $S(\ell + \ell_{\text{bin}}, \ell)$ [4]. This number is reasonable if $\ell_{\text{bin}} = 2$. For instance, $S(4, 2) = 7$, $S(5, 3) = 25$, $S(6, 4) = 65$, $S(7, 5) = 140$. Thus, we select that value of ℓ_{bin} for the applications.

It is important to note that the clustering before splitting, \mathbf{C} , is described by one of the partitions of \mathcal{P} , that is $\mathbf{C} \in G(\mathbf{C})$. Therefore, the best possible merge can return to the clustering before the perturbation step, which guarantees that *Perturb* does not increase the quantization error (Proposition 4).

Perturbation intensity

In our implementation, the clustering perturbation intensity is set to decrease with time. Looking at the algorithm as a minimizer of the quantization error, this means that the search will be more exploratory at the beginning than at the end, as it is customary in stochastic, global, optimization methods such as simulated annealing. The perturbation intensity is controlled by ℓ_{bin} and p_{bin} . ℓ_{bin} is set equal to 2 to keep the computational complexity of *merge* low enough. p_{bin} decreases with an a priori schedule made of 3 epochs where $p_{\text{bin}} = 0.4$ then 0.2 and 0.1. These values were found by trial and error. Within each epoch, several iterations of $(\text{FindC}, \text{Perturb}, \text{FindR})$ are performed. Before explaining the stopping criterion, we need to describe the last step, *FindR*.

4.3 Finding representatives from clusters

Given a clustering $\mathbf{C} = (C_1, \dots, C_\ell)$, the *FindR* step searches for the associated representatives $\mathbf{R}^*(\mathbf{C}) = (R_1^*(C_1), \dots, R_\ell^*(C_\ell))$ that are optimal in the sense that $R_j^*(C_j) := \arg \min_{r \in \mathcal{R}} \mathcal{W}_p(C_j, r)$. In practice, \mathcal{R} is a parametric family

$\{r(\underline{\eta}), \underline{\eta} \in \mathbb{R}^d\}$. The above minimization is approximated by replacing the distance between the multidimensional distributions $\mathcal{W}_p(C_j, r)$ by the sum over the m dimensions of the p -Wasserstein distances between the marginals. Such an approximation is numerically efficient because the Wasserstein distance in 1D can be easily expressed analytically for two probability measures μ_1 and μ_2 [17]:

$$\mathcal{W}_p(\mu_1, \mu_2) := \left(\int_0^1 |F_1^{-1}(q) - F_2^{-1}(q)|^p dq \right)^{\frac{1}{p}}, \quad (5)$$

where F_1 and F_2 are the cumulative distribution functions. Detailed examples of the *FindR* function with Dirac, normal and uniform distributions are described in Section 5. In these examples, the analytical minimization of the p -Wasserstein distance has only a single local optimum, which is inherently the solution to the problem. Situations with multiple local optima may happen, but the analytical expression of the distance is, in practice, a strong asset in favor of the numerical tractability of *FindR*.

4.4 Implementation aspects

A stopping criterion is implemented in the form of either a minimal change in representatives, or a maximal number of iterations. The minimal change in representatives is measured by the sum over the clusters j of the Euclidean norm between the parameters (η) of the previous representative j and the new one.

For each value of p_{bin} , multiple iterations are performed until convergence is achieved, as explained above. The detailed Augmented quantization algorithm is presented in Appendix F.

5 Toy problems with homogeneous mixtures

5.1 1D uniform example

We consider the sample $S_u = (x_i)_{i=1}^{300} \in \mathbb{R}^{300}$, obtained with a quasi-Monte Carlo method (a Sobol sequence, [9]) to represent the mixture $R_{J_{\text{true}}}^{\text{true}}$ of density $f_{\text{true}} = \frac{1}{3} \mathbb{1}_{[0,1]} + \frac{2}{3} \frac{\mathbb{1}_{[0.3,0.6]}}{0.3}$. The distribution of S_u is shown in Figure 1 and the mixture is defined in Table 1.

We seek to identify two representatives in $\mathcal{R} = \{R_U(a, b), (a, b) \in \mathbb{R}^2, a \leq b\}$, where $R_U(a, b)$ is the measure associated to $\mathcal{U}(a, b)$. In all the applications presented in this article, the p -Wasserstein distance has $p = 2$.

The quantization algorithms start from the two representatives $R_1 = R_U(0, 0.5)$ and $R_2 = R_U(0.5, 1)$. Regarding the *FindR* step, that provides representatives from clusters, we investigate for each cluster C_j and for each dimension

True mixture	Estimated mixture
$R_1^{\text{true}} = R_U(0.01, 1.00)$	$R_1^* = R_U(0.01, 0.99)$
$R_2^{\text{true}} = R_U(0.30, 0.60)$	$R_2^* = R_U(0.30, 0.60)$
$\mathbb{P}(J_{\text{true}} = 1) = 1/3$	$\mathbb{P}(J^* = 1) = 0.33$
$\mathbb{P}(J_{\text{true}} = 2) = 2/3$	$\mathbb{P}(J^* = 2) = 0.67$
$\mathcal{W}_2(S_u, R_{J_{\text{true}}}^{\text{true}}) = 3.6 \times 10^{-3}$	$\mathcal{W}_2(S_u, R_{J^*}^*) = 3.0 \times 10^{-3}$

Table 1: True and estimated mixtures in the uniform 1D test case. $\mathcal{W}_2(S_u, R_{J_{\text{true}}}^{\text{true}}) = \epsilon_2(\mathbf{C}^{\text{true}}, R_{J_{\text{true}}}^{\text{true}})$ is the global error between the true clustering and the true mixture. Similarly, $\mathcal{W}_2(S_u, R_{J^*}^*) = \epsilon_2(\mathbf{C}^*, R_{J^*}^*)$ is the global error between the estimated clustering and the estimated mixture.

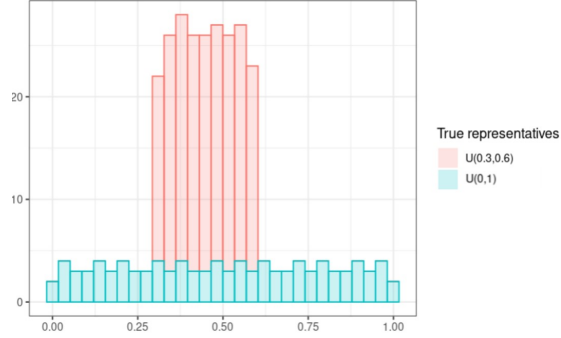


Figure 1: Distribution of S_u .

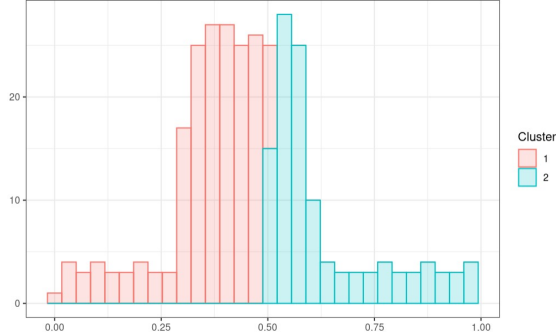


Figure 2: Distribution of two clusters provided by the *FindC* step started from the representatives $R_1 = R_U(0, 0.5)$ and $R_2 = R_U(0.5, 1)$.

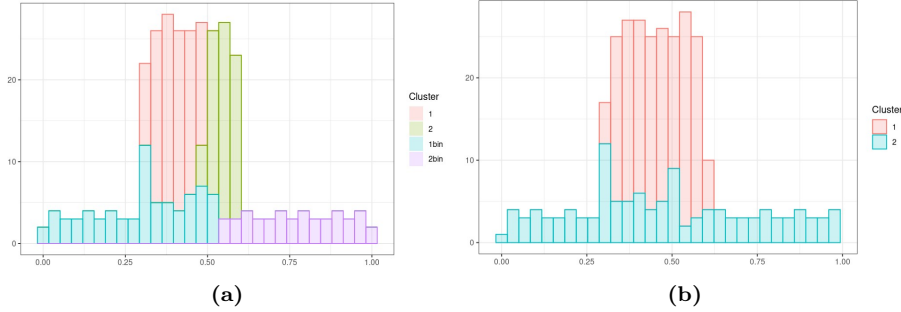


Figure 3: *Perturb* step with $p_{\text{bin}} = 0.4$. Figure 3a shows the *split* into 4 clusters, and Figure 3b is the result of the *merge* phase: clusters 1 and 2 are grouped, clusters 1bin and 2bin are grouped too. Clusters 1bin and 2bin are the elements removed from clusters 1 and 2, respectively.

$k = 1, \dots, m$, ($m = 1$ here) the best parameters $(a_j^k, b_j^k) \in \mathbb{R}^2$ minimizing $\mathcal{W}_2(C_j^k, R_U(a_j^k, b_j^k))$, where $C_j^k = \{x^k : (x^1, \dots, x^m) \in C_j\}$. Denoting Q_j^k the empirical quantile function of C_j^k , the optimal uniform representative can be explicitly calculated as

$$a_j^k = \int_0^1 Q_j^k(q)(-6q + 4) dq, \quad \text{and} \quad b_j^k = \int_0^1 Q_j^k(q)(6q - 2) dq.$$

The first *FindC* step of Algorithm 2 yields the two clusters shown in Figure 2. The *Perturb* step is illustrated in Figure 3 with $p_{\text{bin}} = 0.4$. Then the *FindR* function provides two new representatives, $R_1 = R_U(0.31, 0.60)$ and $R_2 = R_U(0.03, 0.93)$. This single iteration is enough to get close to the representatives of the investigated mixture. At the completion of the other iterations, the estimated mixture $R_{j^*}^*$ reported in Table 1 is found. This mixture is represented in Figure 4b, with the optimal clusters illustrated in Figure 4a. The optimal quantization error is $\mathcal{E}_2(\mathbf{C}^*, \mathbf{R}^*) = 4.4 \times 10^{-3}$ and the global error is

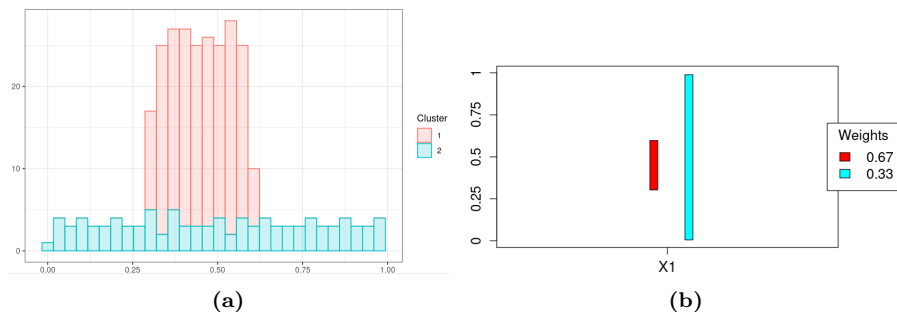
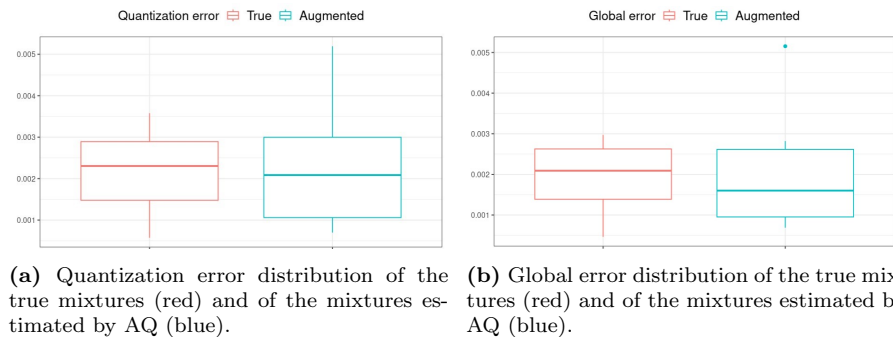


Figure 4: 4a: The optimal clusters estimated by AQ. 4b: The optimal representatives and their weights. Each color is associated to a representative, and the support of the uniform distributions are plotted as a vertical bar.



(a) Quantization error distribution of the true mixtures (red) and of the mixtures estimated by AQ (blue). **(b)** Global error distribution of the true mixtures (red) and of the mixtures estimated by AQ (blue).

Figure 5: Distributions of the errors in the uniform test case.

$\epsilon_2(\mathbf{C}^*, \mathbf{R}^*) = 3.0 \times 10^{-3}$. As shown in Table 1, this global error is slightly lower than that between the true mixture and the sample. Thus, the algorithm finds a solution whose accuracy is of the order of the sampling error.

To test the robustness of the method, the previous experiment is repeated with 15 other samples made of 300 points obtained from Sobol sequences that represent mixtures of respective densities $f_i = p_i \frac{\mathbb{1}_{[a_i, b_i]}}{b_i - a_i} + (1 - p_i) \frac{\mathbb{1}_{[c_i, d_i]}}{d_i - c_i}$, with $a_i, b_i, c_i, d_i, p_i \in [0, 1]$ sampled such that $b_i > a_i$ and $d_i > c_i$. The resulting distributions of the quantization errors and the global errors and the comparison with the errors of the true mixtures are shown in Figure 5. The errors are low throughout the repetitions. For example, the median quantization error, which falls below 2×10^{-3} , is smaller than the one achieved with the true mixtures. The distribution of the global errors have a similar pattern. The evolution of the quantization error throughout the iterations is described in Appendix G.

5.2 A mixture of Dirac example

We now assume that the representatives are delta Dirac measures, which corresponds to the classical quantization problem: we have $\mathcal{R} = \{\delta_\gamma, \gamma \in \mathcal{X}\}$, where δ_γ is the Dirac measure at the point γ .

The *FindC* procedure described in Section 4.1 is equivalent to the computation of the Voronoi cells in Lloyd's algorithm. From $\mathbf{R} = (\delta_{\gamma_1}, \dots, \delta_{\gamma_\ell})$, it provides $\mathbf{C} = (C_1, \dots, C_\ell)$ with $C_j = \{x : j = \arg \min_{j'} \|x - \gamma_{j'}\|\}$.

The *FindR* step of Section 4.3 amounts to finding, for all clusters j , γ_j minimizing

$$\mathcal{W}_2(\gamma, C_j)^2 = \frac{1}{\text{card}(C_j)} \sum_{x \in C_j} \|x - \gamma\|^2.$$

The solution is, for $j \in \mathcal{J}$,

$$\gamma_j = \frac{1}{\text{card}(C_j)} \sum_{x \in C_j} x.$$

With Dirac representatives, like for *FindC*, *FindR* degenerates into a step of Lloyd's algorithm. Note that it is equivalent to optimize the sum of the Wasserstein distances on each marginal, as proposed in Section 4.3.

In the Dirac case, the Augmented Quantization is identical to the classical K-means quantization, but with an additional step of clusters perturbation. We now investigate the effect of this operation.

Lloyd's algorithm and AQ are compared on 500 different samples of 20 points with 20 starting clusters centers tested for each sample, which means a total of 2×10^4 runs. The samples are i.i.d. realizations of a uniform distribution in $[0, 1]^2$, and the quantization is performed with two representatives. Figure 6 shows one example of the results. For each of these tests, the quantization errors (Equation (1)) are computed for the two methods, and are denoted $\mathcal{E}_{\text{Lloyd}}$ and \mathcal{E}_{AQ} for Lloyd's algorithm and AQ, respectively.

The distribution of the difference, $\frac{\mathcal{E}_{\text{Lloyd}} - \mathcal{E}_{\text{AQ}}}{\mathcal{E}_{\text{Lloyd}}} \times 100$, is provided in Figure 7. In 44% of the tests, both methods have the same quantization error. AQ outperforms Lloyd's algorithm (as characterized by a negative relative difference) in 50% of the cases.

The median of the improvement of AQ over Lloyd is 3.1%, and the third quartile is 7.7%. Thanks to the cluster perturbation, the Augmented Quantization produces significantly better results than K-means in the Dirac case.

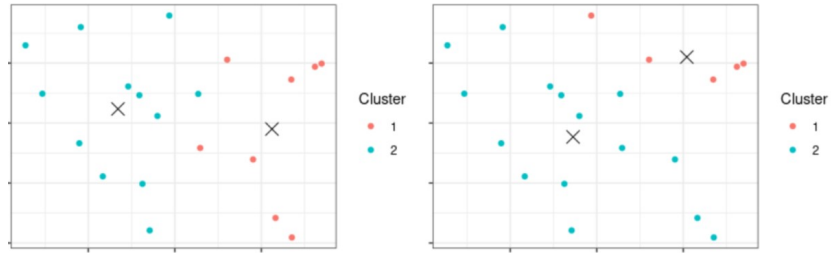


Figure 6: An example of the optimal clusters (red and blue dots) and their centroids (black crosses) obtained with Lloyd's algorithm (left) and AQ (right). Both algorithms were started with the same representatives (i.e., here, cluster centers). The quantization error is 0.28 with Lloyd's algorithm and 0.25 with AQ.

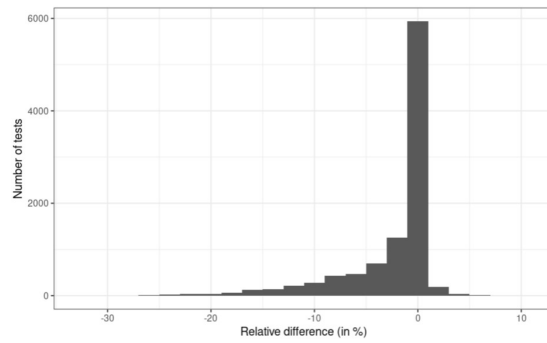


Figure 7: Distribution of the relative difference (in %) between the quantization errors of Lloyd's algorithm and AQ. Negative values correspond to a better performance of AQ.

5.3 A Gaussian mixture example

The Gaussian mixture models, denoted GMM and estimated with the EM algorithm are very popular when it comes to identifying Gaussian representatives. In the following example, we compare the Augmented Quantization with this well-known GMM in one dimension. The representatives belong to $\mathcal{R} = \{R_N(\mu, \sigma^2), (\mu, \sigma) \in \mathbb{R}^2\}$ where R_N is the measure associated to $\mathcal{N}(\mu, \sigma^2)$.

The *FindR* step is the minimization of $\mathcal{W}_2(C_j^k, R_N(\mu_j^k, (\sigma_j^k)))$, for each cluster C_j and each dimension $k = 1, \dots, m$, ($m = 1$ here). It leads to

$$\begin{cases} \mu_j^k &= \int_0^1 Q_j^k(q) dq = \frac{1}{\text{card}(C_j^k)} \sum_{x \in C_j^k} x \\ \sigma_j^k &= \frac{\int_0^1 Q_j^k(q) \text{erf}^{-1}(2q-1) dq}{\sqrt{2} \int_0^1 (\text{erf}^{-1}(2q-1))^2 dq} \end{cases}$$

where erf is the error function defined by $\text{erf}(z) = \frac{2}{\sqrt{\pi}} \int_0^z \exp(-t^2) dt$.

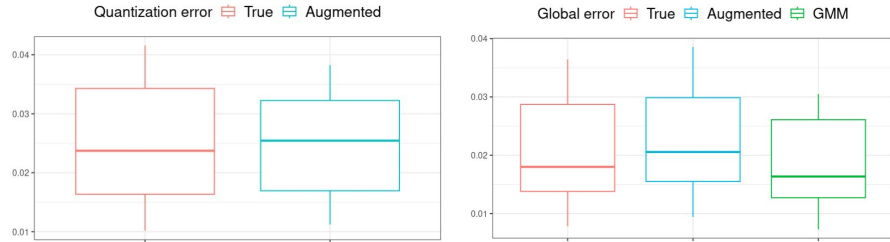
It is important to note that this *FindR* procedure leads to representatives with independent marginals, while GMM can describe a covariance structure.

We consider a family of samples $(S_g^i)_{i=1}^{15}$, made of 400 points obtained with Gaussian transformations of Sobol sequences. They represent mixtures of density $f_i(x) = p_i \frac{1}{\sigma_i^1 \sqrt{2\pi}} \exp(-(\frac{x-\mu_i^1}{\sigma_i^1})^2) + (1-p_i) \frac{1}{\sigma_i^2 \sqrt{2\pi}} \exp(-(\frac{x-\mu_i^2}{\sigma_i^2})^2)$, with $\mu_i^1, \sigma_i^1, \mu_i^2, \sigma_i^2, p_i$ randomly sampled in $[0, 1]$. The distributions of the quantization and global errors are provided in Figure 8. The *quantization error* can not be computed for GMM, as each element of the sample is assigned to a cluster with a given probability, that is related to the likelihood.

The median of the distribution of our *quantization errors* is very close to the one of the true mixtures, with a lower dispersion, which is very satisfactory. The distributions of our *global errors* is similar as well, highlighting that the additional error is much lower than the sampling error. The median of the distribution of our *quantization errors* and *global errors* are very close to the ones of the true mixtures, and the dispersion of which is very satisfactory. Our obtained *quantization errors* have even less variability, The GMM scheme, on the other hand, identifies slightly better mixtures to represent the samples. We can note that these errors are higher than for the uniform mixture. Indeed, the samples obtained by quasi-Monte Carlo methods are closer to their targeted distribution in the uniform case compare to the Gaussian one.

Figure 9 displays the example of a sample S_g^t in the previously introduced family of samples, more specifically the one corresponding to the median *global error* obtained with AQ.

Table 2 summarizes the results. Even though GMM finds a closer distribution, Figure 10b illustrates that it is really close to the one obtained with Augmented Quantization. Figure 10a shows that the clusters identified by AQ are promising when comparing their distributions to their representatives. To conclude, both methods identify relevant sub-distributions, but GMM remains slightly better here as it is less general than AQ: it would not allow mixing Gaussian distribution with Dirac or uniform ones.



(a) Distribution of the *quantization errors* for the true mixtures (red) and the one obtained with AQ (blue). (b) Distribution of the *global errors* for the true mixtures (red), the one obtained with AQ (green), and the GMM approach (blue).

Figure 8: Distributions of the errors in the Gaussian case.

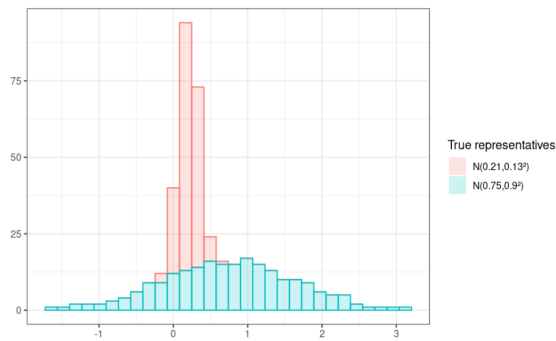
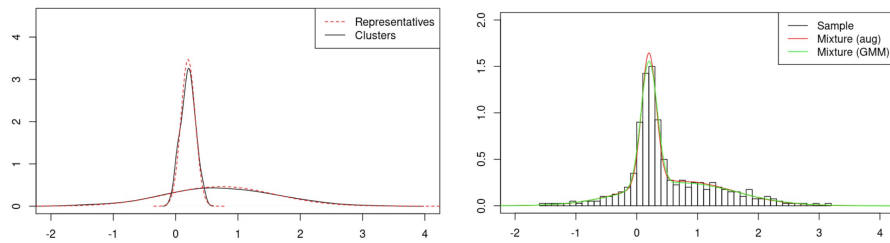


Figure 9: Distribution of S_g^t



(a) Density of the optimal clusters and their representatives estimated with AQ for the sample S_g^t . (b) Distribution of the sample S_g^t (black histogram), the optimal Gaussian mixture obtained with AQ (red) and the Gaussian mixture obtained with GMM algorithm (green).

Figure 10: Optimal mixture estimated with AQ and comparison with GMM.

True mixture	AQ mixture	GMM Mixture
$R_1^{\text{true}} = R_N(0.21, 0.13^2)$	$R_1^* = R_N(0.20, 0.12^2)$	$R_1^{\text{GMM}} = R_N(0.20, 0.13^2)$
$R_2^{\text{true}} = R_N(0.75, 0.9^2)$	$R_2^* = R_N(0.72, 0.86^2)$	$R_2^{\text{GMM}} = R_N(0.74, 0.89^2)$
$\mathbb{P}(J_{\text{true}} = 1) = 0.45$	$\mathbb{P}(J^* = 1) = 0.4$	$\mathbb{P}(J_{\text{GMM}} = 1) = 0.38$
$\mathbb{P}(J_{\text{true}} = 2) = 0.55$	$\mathbb{P}(J^* = 2) = 0.6$	$\mathbb{P}(J_{\text{GMM}} = 2) = 0.62$
$W_2(S_g^t, R_{J_{\text{true}}}^{\text{true}}) = 2.9 \times 10^{-3}$	$W_2(S_g^t, R_{J^*}^*) = 3.3 \times 10^{-2}$	$W_2(S_g^t, R_{J_{\text{GMM}}}^{\text{GMM}}) = 2.9 \times 10^{-3}$

Table 2: True and estimated mixture with AQ and with GMM in the Gaussian test case S_g^t in 1D. $W_2(S_g^t, R_{J_{\text{true}}}^{\text{true}})$, $W_2(S_g^t, R_{J^*}^*)$, and $W_2(S_g^t, R_{J_{\text{GMM}}}^{\text{GMM}})$ are the global errors between the clusterings and the mixtures.

6 An hybrid mixture test case

Here, we tackle the hybrid case of a hybrid mixture with a Gaussian and a uniform representative to illustrate the possibilities of the method compared to existing schemes such as GMM. We consider a sample S_{hyb} of 350 points, displayed in Figure 11a, distributed to represent a mixture of density $f_{\text{hyb}} = \frac{1}{3} \mathbb{1}_{[0.2, 0.5]} + \frac{2}{3} \frac{1}{0.2\sqrt{2\pi}} \exp(-(\frac{x-0.6}{0.2})^2)$. Figure 11b shows that the two representatives are well identified by AQ, leading to a *quantization error* of 8.3×10^{-3} and of a *global error* equal to 7.6×10^{-3} . GMM is not designed to investigate this type of distributions.

To ensure the robustness of the method, a family of samples $(S_{\text{hyb}}^i)_{i=1}^{15}$ of size 350 is considered and a comparison between the true mixtures and the obtained ones is provided in Figure 12. These boxplots illustrate that the identified mixtures represent well the samples, with distributions of errors near the distributions of the errors obtained with the true mixtures. Again, the additional error is very small compared to the sampling error due to limited size of the samples.

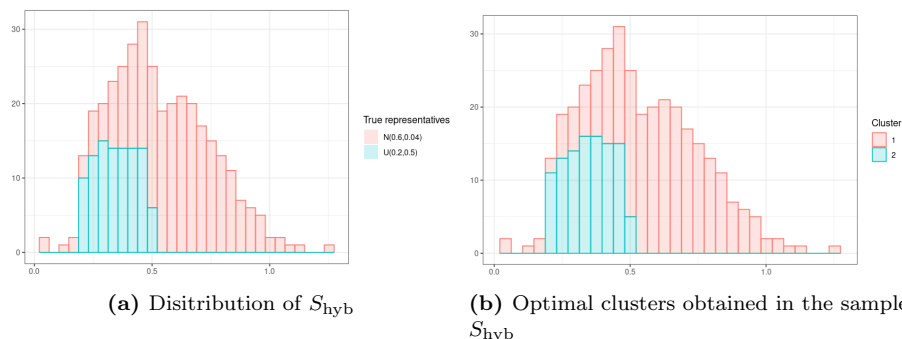
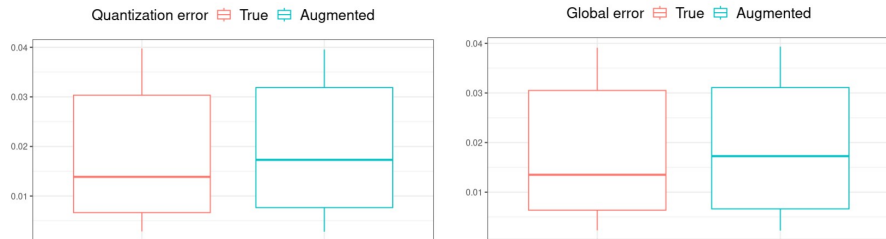


Figure 11: Illustration of the hybrid case of a Gaussian and a uniform representative.



(a) Distribution of the *quantization errors* for the true mixtures (red) and the one obtained with AQ (blue). (b) Distribution of the *global errors* for the true mixtures (red) and the one estimated with AQ (blue).

Figure 12: Distributions of the errors in the hybrid case.

7 Application to river flooding

Augmented Quantization allows to approximate a distribution with mixtures of various probability measures, including uniform and Dirac. A possible application is to perform sensitivity analysis on an industrial simulator.

When dealing with industrial problems with random inputs, a possible method to visualize information on the probability distribution of the output is to perform classical quantization [23]. The objective is to identify prototype outputs with an associated probability mass which is the membership probability of the induced Voronoï cell. This set of prototypes and their mass describe the continuous distribution of the outputs by bringing an discrete approximation of it. This study can be really relevant when discussing to stakeholders.

A natural need after this investigation is to work on the distribution of the inputs leading to each prototype output. More precisely, to have an approximation of the multivariate distribution of the inputs in each Voronoï cell can bring information on the causes of the different output regimes. For instance, if one of the input variables has the same marginal distribution in one Voronoï cell than its overall distribution, it suggests that this variable has no influence in the related regime of output. Associating a multivariate visualization to this marginal analysis can help analyzing the interaction between the variables.

In this study, we have chosen to investigate the probabilistic distribution of flood maps and their related inputs. Specifically, our case study focuses on a section of the Loire River near Orléans, France, which is flanked by levees on both banks and has a history of significant flooding in the 19th century, including historical breaches [11] in our study area illustrated in Figure 13 .

To simulate the river flow of the Loire River between Gien and Jargeau over a distance of 50 km, the Institute for Radiological Protection and Nuclear Safety (IRSN) has built a hydraulic model using open-source TELEMAC-2D computational codes [18]. The model incorporates an upstream hydrograph and a calibration curve as boundary conditions and has been calibrated using well-known flood events by adjusting the roughness coefficients (Strickler coefficients). To simulate breaches, the model considers two parameters: erosion

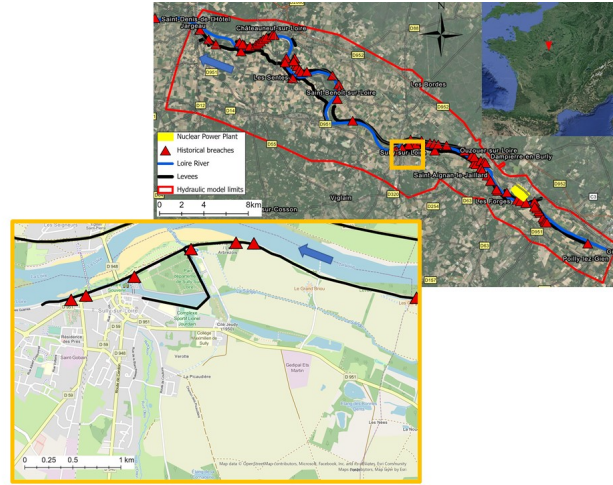


Figure 13: Study area of the flooding test case, including the levees and the historical breaches [15].

rate and breach initiation parameter, also known as control level, which is the water level above the levee. Breaches occur when the water level above the levee reaches the control level.

Due to the large size of the area being modeled, our focus is limited to the left bank sector of the river, specifically Sully-sur-Loire, where we have simulated seven breaches at historical breach sites with lengths corresponding to those of the actual historical breaches.

There are eight input variables in the hydraulic model, considered here as independent:

- Two hydrograph parameters: the maximum flow rate (Q_{\max}) which follows a Generalized extreme value distribution (GEV) and the rise time of the flood (t_m) which follows a truncated log-normal distributions. These distributions were established using the daily flow rate data from the Loire River dataset in Gien.
- Four roughness coefficients (K_s) which follow triangle distributions. As there are calibration coefficients, the distributions cannot be derived from real-world data sets. Therefore, triangular distributions are employed and the mode of these distributions corresponds to the calibration values defined for each roughness area.
- Two breach parameters: the erosion rate (er) which follows a uniform distribution and the overflow (of), indicating the water level above the levee, which follow a uniform distribution.

The approach detailed in [23] is performed based on 1000 flood maps from the hydraulic model and the metamodel build with the R package FunQuant [22].

It yields the 5 prototype maps and their corresponding probabilities provided in Appendix H. Each Voronoi cell represents a flooding regime, and we will specifically focus on analyzing the input distribution associated with the most severe pattern, which has a probability of 5.8×10^{-4} . Based on a preliminary sensitivity analysis, which is not provided in detail here, we have identified a subset of 4 variables for further investigation: Q_m , 2 roughness coefficients denoted K_s^3 and K_s^4 , and the erosion rate er . We have opted to use the rank statistics of the inputs instead of their actual values, as the distribution of these normalized inputs is uniform on each marginal. This transformation allows for straightforward comparison of the input distribution within each Voronoi cell to the overall distribution. To accomplish this, Augmented Quantization is executed within the Voronoi cell with a sample of 500 elements, using 3 representatives that are mixtures of Dirac and uniform distributions with a support of width 0.25, 0.5 or 1 to highlight influential variables: the distribution of a variable that has no impact on this extreme flooding would be a uniform between 0 and 1 while values concentrated around specific values would reveal the influence of a variable. Then, the family of measures here is $\mathcal{R} = \{R(\alpha_1, \dots, \alpha_4, a_1, \dots, a_4, \sigma_1, \dots, \sigma_4)\}$ where $R = R_1 \times \dots \times R_4$ with

$$R_i([x_1, x_2]) = \begin{cases} \alpha_i \frac{\min(x_2, a_i + \frac{\sigma_i}{2}) - \max(x_1, a_i - \frac{\sigma_i}{2})}{\sigma_i} + (1 - \alpha_i) \mathbb{1}_{[x_1, x_2]}(a_i) & \text{if } x_2 > \frac{a_i - \sigma_i}{2} \\ 0 & \text{Otherwise.} \end{cases}$$

with $(\alpha_1, \dots, \alpha_4, a_1, \dots, a_4, \sigma_1, \dots, \sigma_4) \in \{0, 1\}^4 \times [0, 1]^4 \times \{0.25, 0.5, 1\}$.

Figure 14 presents the optimal representatives estimated using AQ, which approximates the distribution of inputs associated with the most severe floodings. Each of the 3 representatives is associated to a color (blue, green and red). A vertical bar is a uniform distribution, and its support of width 0.25, 0.5 or 1 is indicated by the extremities of the bar. A triangle indicates the position of a Dirac. This study emphasizes the significant influence of Q_{\max} , as only Dirac are identified at ranks very close to 1, meaning that only very high values of Q_{\max} result in these extreme events.

The impact of K_{s4} is also evident. Lower values of K_{s4} appear to promote intense flooding, as evidenced by the main representative, the blue one of probability 60%, that exhibits a uniform distribution of width 0.25 between $K_{s4} = 0$ and $K_{s4} = 0.25$. On the other hand, the influence of the low values of K_{s3} is relatively weaker, its main representative (in blue) being a uniform between 0 and 1. However, it has a joint influence with K_{s4} , as observed in the blue and green representatives. This combination accounts for a combined probability mass of approximately 87%, where either K_{s3} or K_{s4} is lower than 0.5.

Interestingly, the high erosion rates er , that represent a important breach, do not seem to have a significant impact on the most severe flooding events, as only 13% of the probability mass is represented by a small uniform: its red representative that has a support between 0.42 and 0.92. The rest of the mass is a uniform between 0 and 1. This can be attributed to the extremely high Q_{\max} values involved, which render the breach impact almost negligible.

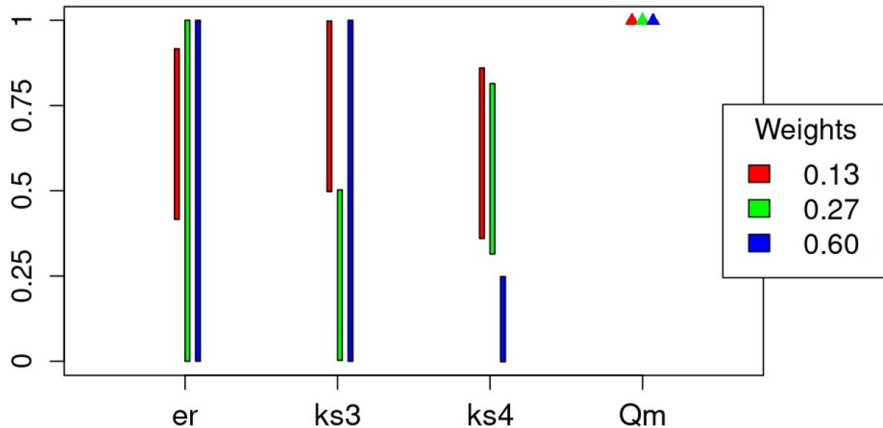


Figure 14: Mixture of Dirac and uniform distributions approximating the distribution of the Voronoi cell 5, associated to the most severe flooding. Each color is associated to a representative. A vertical bar is a uniform distribution, and a triangle indicates the position of a Dirac.

8 Summary and perspectives

This work proposes a new method to build mixture models from a sample $(x_i)_{i=1}^n$. It extends the classical Lloyd’s algorithm used in quantization to generate Dirac mixtures. In Lloyd’s algorithm, random elements of the sample are selected as the initial positions of the Dirac measures, and the clusters are associated iteratively with these elements (step *update clusters*), followed by updating the positions of the Diracs by computing the centroids of these clusters (step *update centroids*). The optimal centroids obtained minimize the quantization error of Equation 1. The problem can be formulated with the Wasserstein distance to extend it to all types of distributions, discrete or continuous, with finite or infinite support. That builds a mixtures of probability measures called representatives. The *update clusters* and *update representatives* steps are adapted with the Wasserstein distance, and an additional step of cluster perturbation is added to make the approach more exploratory.

The overall algorithm addresses the common problem of mixture models but in a more general formulation. K-means quantization, which is used for Dirac mixtures, or the Expectation-Maximization algorithm, based on maximum likelihood estimation, are more restrictive. Our method still uses the clustering approach that reduces the complexity of the problem compared to directly optimizing the parameters of the mixture (i.e., parameters of the representatives and their probabilistic weights). For example, the number of parameters to optimize for three uniform representatives in 3D is 20 with direct optimization but reduced to 6 parameters by clusters here. The quantization error associated to this clustering scheme remains consistent, and a low error guarantees a mixture

with a distribution close to the data.

Although the results obtained are promising, several areas of improvement are worth exploring.

Tuning of the p_{bin} parameters. The initial step in the perturbation of clusters involves dividing the ℓ_{bin} clusters C_j with the highest *local error* $w_p(C_j)$ into two clusters, one named the “bin”, which contains the worst elements of the clusters. The number of elements added to this bin is determined by a proportion of the initial cluster size denoted as p_{bin} , which is a crucial algorithmic parameter. In our study, p_{bin} is pre-selected before each division, and there is no active learning process to adjust it. An improved version of the method could be to intelligently select the proportion p_{bin} . One approach could be to examine the behavior of $\mathcal{E}_p(C_j^{\text{split}}(x))$ (Section 4.2) to detect a cut-off point where the best transfer from the cluster to the bin is no longer relevant. However, identifying such a cut-off point can be challenging, and it does not guarantee that it will result in the best perturbation since the merge step is not taken into account in this study.

Active learning of the number of representatives. In the method described here, the merge step is carried out to maintain a constant number of clusters, denoted as ℓ . This is useful when there is a specific requirement for this number or a strong prior knowledge of the data structure. However, in a more general scenario, cluster perturbation could be adapted to intentionally modify the number of clusters based on the Wasserstein distances between the clusters (including the bins) and their representatives. For example, some merges could significantly increase the quantization error, indicating that the number of clusters may need to be increased. While this operation is worth exploring, it would likely add computational complexity to the method.

Computational burden. The methodology presented in this article aims to be innovative in its approach to computing Wasserstein distances, which provides a general formulation of the classical quantization problem. However, at present, the computational cost of the methodology restricts the sample size under investigation to less than several thousand due to the execution of greedy algorithms. The split step, in particular, incurs dominant complexity, as the selection of the optimal element x^* to transfer from the cluster to the bin necessitates computing Wasserstein distances for all possible transfers. To alleviate the computational burden, it may be worthwhile to investigate batch transfer approaches or considering only a subset of the possible transfers, although this may reduce precision. As the overall complexity depends on the the complexity of the Wasserstein distance, it may be possible to approximate its computation using sliced Wasserstein distance [14].

References

- [1] Murray Aitkin and Donald B. Rubin. “Estimation and Hypothesis Testing in Finite Mixture Models”. In: *Journal of the Royal Statistical Society. Series B (Methodological)* 47.1 (1985), pp. 67–75. ISSN: 00359246. URL: <http://www.jstor.org/stable/2345545> (visited on 11/22/2022).
- [2] Brent Burch and Jesse Egbert. “Zero-inflated beta distribution applied to word frequency and lexical dispersion in corpus linguistics”. In: *Journal of Applied Statistics* 47.2 (2020). PMID: 35706513, pp. 337–353. DOI: 10.1080/02664763.2019.1636941.
- [3] Marco Capó, Aritz Pérez, and Jose A. Lozano. “An Efficient Split-Merge Re-Start for the KK-Means Algorithm”. In: *IEEE Transactions on Knowledge and Data Engineering* 34.4 (2022), pp. 1618–1627. DOI: 10.1109/TKDE.2020.3002926.
- [4] O-Yeat Chan and Dante V. Manna. “Congruences for Stirling Numbers of the Second Kind”. In: 2009.
- [5] Frank Dellaert. “The Expectation Maximization Algorithm”. In: (July 2003).
- [6] Qiang Du, M. Emelianenko, and Lili Ju. “Convergence of the Lloyd Algorithm for Computing Centroidal Voronoi Tessellations”. In: *SIAM Journal on Numerical Analysis* 44 (Jan. 2006), pp. 102–119. DOI: 10.1137/040617364.
- [7] Nicolas Fournier and Arnaud Guillin. *On the rate of convergence in Wasserstein distance of the empirical measure*. 2013. arXiv: 1312.2128 [math.PR].
- [8] R.M. Gray and D.L. Neuhoff. “Quantization”. In: *IEEE Transactions on Information Theory* 44.6 (1998), pp. 2325–2383. DOI: 10.1109/18.720541.
- [9] Stephen Joe and Frances Y Kuo. “Notes on generating Sobol sequences”. In: *ACM Transactions on Mathematical Software (TOMS)* 29.1 (2008), pp. 49–57.
- [10] Clément Levrard. “Quantization/clustering: when and why does k-means work?” working paper or preprint. Jan. 2018. URL: <https://hal.archives-ouvertes.fr/hal-01667014>.
- [11] Jean Maurin et al. “Études de dangers des digues de classe A de la Loire et de ses affluents – retour d’expérience”. In: June 2013.
- [12] Quentin Mérigot, Filippo Santambrogio, and Clément Sarrazin. “Non-asymptotic convergence bounds for Wasserstein approximation using point clouds”. In: *Advances in Neural Information Processing Systems* 34 (2021), pp. 12810–12821.
- [13] See Ng, Thriyambakam Krishnan, and G. McLachlan. “The EM algorithm”. In: *Handbook of Computational Statistics: Concepts and Methods* (Jan. 2004). DOI: 10.1007/978-3-642-21551-3_6.

- [14] Sloan Nietert et al. “Statistical, Robustness, and Computational Guarantees for Sliced Wasserstein Distances”. In: *Advances in Neural Information Processing Systems*. Ed. by S. Koyejo et al. Vol. 35. Curran Associates, Inc., 2022, pp. 28179–28193. URL: https://proceedings.neurips.cc/paper_files/paper/2022/file/b4bc180bf09d513c34ecf66e53101595-Paper-Conference.pdf.
- [15] OpenStreetMap contributors. *Planet dump retrieved from https://planet.osm.org. https://www.openstreetmap.org*. 2017.
- [16] Gilles Pagès. *Introduction to optimal vector quantization and its applications for numerics*. Tech. rep. 54 pages. July 2014. URL: <https://hal.archives-ouvertes.fr/hal-01034196>.
- [17] Victor M. Panaretos and Yoav Zemel. “Statistical Aspects of Wasserstein Distances”. In: *Annual Review of Statistics and Its Application* 6.1 (2019), pp. 405–431. DOI: 10.1146/annurev-statistics-030718-104938.
- [18] Lucie Pheulpin, Antonin Migaud, and Nathalie Bertrand. “Uncertainty and Sensitivity Analyses with dependent inputs in a 2D hydraulic model of the Loire River”. In: June 2022. DOI: 10.3850/IAHR-39WC2521716X20221433.
- [19] D. Pollard. “Quantization and the method of k-means”. In: *IEEE Transactions on Information Theory* 28.2 (1982), pp. 199–205. DOI: 10.1109/TIT.1982.1056481.
- [20] Ludger Rueschendorf. “The Wasserstein Distance and Approximation Theorems”. In: *Probability Theory and Related Fields* 70 (Mar. 1985), pp. 117–129. DOI: 10.1007/BF00532240.
- [21] Shokri Z. Selim and M. A. Ismail. “K-Means-Type Algorithms: A Generalized Convergence Theorem and Characterization of Local Optimality”. In: *IEEE Transactions on Pattern Analysis and Machine Intelligence* PAMI-6.1 (1984), pp. 81–87. DOI: 10.1109/TPAMI.1984.4767478.
- [22] Charlie SIRE. *The FunQuant package*. 2023. URL: <https://github.com/charliesire/FunQuant>.
- [23] Charlie Sire et al. “Quantizing rare random maps: application to flooding visualization”. In: *Journal of Computational and Graphical Statistics* 0 (2023), pp. 1–31. DOI: 10.1080/10618600.2023.2203764. URL: <https://doi.org/10.1080/10618600.2023.2203764>.
- [24] Ramesh Sridharan. “Gaussian mixture models and the EM algorithm”. In: 2014.
- [25] Onur Teymur et al. “Optimal Quantisation of Probability Measures Using Maximum Mean Discrepancy”. In: (Oct. 2020).
- [26] C. Villani. *Optimal Transport: Old and New*. Grundlehren der mathematischen Wissenschaften. Springer Berlin Heidelberg, 2016. ISBN: 9783662501801. URL: <https://books.google.fr/books?id=5p8SDAEACAAJ>.

- [27] Sidney J. Yakowitz and John D. Spragins. “On the Identifiability of Finite Mixtures”. In: *The Annals of Mathematical Statistics* 39.1 (1968), pp. 209–214. DOI: 10.1214/aoms/1177698520. URL: <https://doi.org/10.1214/aoms/1177698520>.

A Expectation-Maximization with uniform mixtures

A.1 Lower and upper bounds

Let us consider (x_i, \dots, X^n) i.i.d. random variables, and a realization $S_{EM} = (x_i)_i^n$. We want to approximate the distribution by a mixture with two representatives associated to $U(a_1, b_1)$ and $U(a_2, b_2)$. We want to optimize the bounds and the weights p_1 and $p_2 = 1 - p_1$ of the representatives by maximum likelihood, as in the Expectation maximization algorithm. Let us denote $\theta = (a_1, b_1, a_2, b_2, p_1)$.

The likelihood function is

$$\mathcal{L}(\theta) = \prod_{i=1}^n \left(p_1 \frac{\mathbb{1}_{[a_1, b_1]}(x_i)}{b_1 - a_1} + (1 - p_1) \frac{\mathbb{1}_{[a_2, b_2]}(x_i)}{b_2 - a_2} \right)$$

Thus, the optimization of $\mathcal{L}(\theta)$ will lead to $\min\{a_1, a_2\} = \min x_i$ and $\max\{b_1, b_2\} = \max x_i$.

Let us suppose the distribution of S_{EM} is the one provided in Figure 16.

It appears clearly that the distribution is close to a mixture of a uniform $\mathcal{U}(0, 1)$ and a uniform $\mathcal{U}(0.7, 0.9)$. However the few elements at -0.2 would impose a lower bound of the representatives at this value when optimizing through maximum likelihood.

A.2 Details of the Expectation-Maximization approach

The EM algorithm starts with an initial set of parameters $\theta^{(0)}$, and aims at converging to an optional θ^* maximizing likelihood. It is based on the introduction of a latent random variable $Z = (Z_1, \dots, Z_n)$ indicating to which representative the elements are assigned.

Thus, the E-step perform a soft-assignment, attributing to each sample element a probability of being associated to each representatives j [13]:

$$\text{for } i = 1 : n, \mathbb{P}(Z_i = j \mid \theta) = p_{Z_i|x_i}(j \mid x_i; \theta) = \frac{p_{x_i|Z_i}(x_i \mid Z_i = j; \theta)p_j}{P_{x_i}(x_i \mid \theta)}$$

The M-step estimates new parameters θ^{new} increasing the likelihood [24]:

$$\theta^{\text{new}} = \arg \max_{\theta} \mathbb{E}_Z (p_{X|Z}(x \mid Z, \theta)p_Z(Z))$$

Let us suppose that the sample S_{EM} is the one illustrated in Figure 16, but without the points below 0. Thus, its distribution is almost the one of a mixture of two representatives $\mathcal{U}(0, 1)$ and $\mathcal{U}(0.7, 0.9)$. Let us run an iteration of the EM algorithm and analyse how it works with uniform mixtures.

Let us start with the following initial parameters: $a_1 = \min x_i, b_1 = 0.5, a_2 = 0.5, b_2 = \max(x_i)_i^n, p_1 = p_2 = 0.5$.

The E-step assigns a probability to each pair of element and representative.

$$\text{For } i = 1 : n \text{ and } j = 1 : 2, \mathbb{P}(Z_i = j) = \frac{\frac{\mathbb{1}_{[a_j, b_j]}(x_i)}{b_j - a_j}}{\frac{\mathbb{1}_{[a_1, b_1]}(x_i)}{b_1 - a_1} + \frac{\mathbb{1}_{[a_2, b_2]}(x_i)}{b_2 - a_2}}$$

Thus, if $x_i < 0.5$, $\mathbb{P}(Z_i = 1) = 1$ and $\mathbb{P}(Z_i = 2) = 0$. If $x_i > 0.5$, $\mathbb{P}(Z_i = 1) = 0$ and $\mathbb{P}(Z_i = 2) = 1$.

The M-step aims at determining parameters $\theta^{\text{new}} = (a_1^{\text{new}}, b_1^{\text{new}}, a_2^{\text{new}}, b_2^{\text{new}}, p_1^{\text{new}})$.

$$\forall \theta, \mathbb{E}_Z (p_{X|Z}(x | Z, \theta) p_Z(Z)) = \prod_{i, x_i < 0.5} p_1 \frac{\mathbb{1}_{[a_1, b_1]}(x_i)}{b_1 - a_1} \prod_{i, x_i > 0.5} (1 - p_1) \frac{\mathbb{1}_{[a_2, b_2]}(x_i)}{b_2 - a_2}.$$

The optimization will lead to $a_1 = \min x_i, b_1 = \min_{i, x_i < 0.5} x_i, a_2 = \min_{i, x_i > 0.5} x_i, b_2 = \max x_i$.

It appears that the clusters will not evolve through the iterations and the algorithm will not find the optimal representatives.

B Removing clusters perturbation step

Here we perform AQ without the clusters perturbation, with the toy problem described in Section 5.1, starting from two representatives $R_1 = R_U(0, 0.5)$ and $R_2 = R_U(0.5, 1)$.

Figure 15 shows the clusters obtained after each of the first 9 iterations. The algorithm is rapidly stuck in a configuration far from the optimal quantization, with representatives around $R_U(0.26, 0.93)$ and $R_U(0.19, 0.63)$.

The obtained quantization error here is 4.0×10^{-2} , more than 10 times higher than the optimal quantization error obtained with Augmented Quantization including clusters perturbation, equal to 4.4×10^{-3} (see Section 5.1).

C Proof of Proposition 1

Let $\mathbf{R} = (R_1, \dots, R_\ell)$ be ℓ probability measures and $\mathbf{C} = (C_1, \dots, C_\ell)$ be ℓ disjoint clusters of points $\in \mathcal{X} \subset \mathbb{R}^d$. In addition, let us denote

- $n_j = \text{card}(C_j)$ for $j \in \mathcal{J}$, and $n = \sum_{j=1}^{\ell} n_j$
- μ_C^j the empirical measure associated to C_j
- $\mathbf{\Pi}_j$ as the set of all coupling probabilities π_j on $\mathcal{X} \times \mathcal{X}$ such that $\int_{\mathcal{X}} \pi_j(x, x') dx = R_j(x')$ and $\int_{\mathcal{X}} \pi_j(x, x') dx' = \mu_C^j(x)$
- $\pi_j^* = \inf_{\pi_j \in \mathbf{\Pi}_j} \int_{\mathcal{X} \times \mathcal{X}} \|x - x'\|^p \pi_j(x, x')$

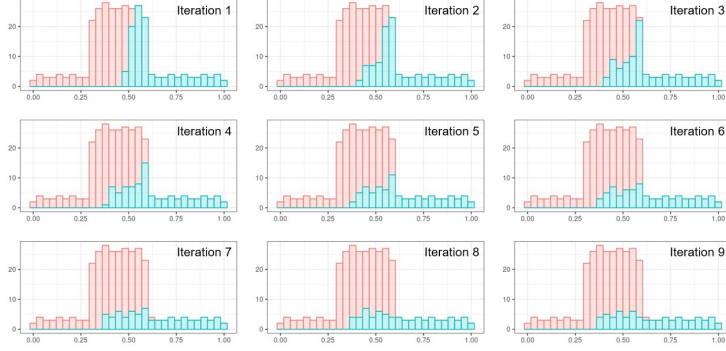


Figure 15: Distribution of clusters 1 and 2 in the 1D uniform case when performing the method without the clusters perturbation.

- $p_j = \frac{n_j}{n}$
- μ_{UC} the empirical measure associated to $\bigcup_{j=1}^{\ell} C_j$
- $\mathbf{\Pi}_{\text{global}}$ as the set of all coupling probabilities π on $\mathcal{X} \times \mathcal{X}$ such that $\int_{\mathcal{X}} \pi(x, x') dx = R_J(x')$ and $\int_{\mathcal{X}} \mathbf{\Pi}_j(x, x') dx' = \mu_{UC}(x)$

By definition of R_J , we have $R_J = \sum_{k=1}^{\ell} p_j R_j$. Similarly, we have $\mu_{UC} = \sum_{k=1}^{\ell} p_j \mu_C^j$.

$$\begin{aligned}
\mathcal{E}_p(\mathbf{C}, \mathbf{R}) &= \left(\sum_j^{\ell} \frac{n_j}{n} \mathcal{W}_p(C_j, R_j)^p \right)^{\frac{1}{p}} \\
&= \left(\sum_{j=1}^{\ell} \frac{n_j}{n} \int_{\mathcal{X} \times \mathcal{X}} \|x - x'\|^p \pi_j^*(dx, dx') \right)^{\frac{1}{p}} \\
&= \left(\int_{\mathcal{X} \times \mathcal{X}} \|x - x'\|^p \sum_{j=1}^{\ell} p_j \pi_j^*(dx, dx') \right)^{\frac{1}{p}} \\
&= \left(\int_{\mathcal{X} \times \mathcal{X}} \|x - x'\|^p \tilde{\pi}(dx, dx') \right)^{\frac{1}{p}}
\end{aligned}$$

with $\tilde{\pi} = \sum_{j=1}^{\ell} p_j \pi_j^*$.
Since for $j \in \mathcal{J}$, $\pi_j^* \in \mathbf{\Pi}_j$,

$$\begin{aligned}
\int_{\mathcal{X}} \tilde{\pi}(dx, x') &= \sum_{j=1}^{\ell} p_j \int_{\mathcal{X}} \pi_j^*(dx, x') \\
&= \sum_{j=1}^{\ell} p_j R_j(x') dx \\
&= R_J(x') .
\end{aligned}$$

Similarly, $\int_{\mathcal{X}} \tilde{\pi}(x, x') dx' = \mu_{UC}(x)$. This shows that $\tilde{\pi} \in \mathbf{\Pi}_{\text{global}}$.
Finally,

$$\begin{aligned}
\epsilon_p(\mathbf{C}, \mathbf{R}) &= \mathcal{W}_p\left(\bigcup_{j=1}^{\ell} C_j, R_J\right) \\
&= \inf_{\pi \in \mathbf{\Pi}_{\text{global}}} \left(\int_{\mathcal{X} \times \mathcal{X}} \|x - x'\|^p \pi(dx, dx') \right)^{\frac{1}{p}} \\
&\leq \mathcal{E}_p(\mathbf{C}, \mathbf{R}) \quad \square
\end{aligned}$$

D Proof of clustering consistency (Proposition 3)

We recall and complete our notations used to discuss clustering:

- The representative mixtures are $(R_1, \dots, R_{\ell}) \in \mathcal{R}_s^{\ell}$
- J is a random variable with $\forall j \in \mathcal{J}, P(J = j) = p_j$
- $(X_k)_{k=1}^n$ are i.i.d. data samples and X_k has probability measure R_J
- $(J_i)_{i=1}^N$ are i.i.d. samples with same distribution as J
- $(Y_i)_{i=1}^N$ are i.i.d. mixture samples and Y_i has probability measure R_{J_i}
- The index of the representative whose sample is closest to x ,

$$I_N(x) = \arg \min_{i=1, \dots, N} \|x - Y_i\|$$
- The mixture sample the closest to x , $a_N(x) = Y_{I_N(x)}$

$$= \arg \min_{y \in \{Y_1, \dots, Y_N\}} \|x - y\|$$
- The k -th data sample that is assigned to cluster j , $\tilde{X}_{k,N}^{(j)} = X_k \mid J_{I_N(X_k)} = j$. This of course does not mean that the k -th sample will belong to cluster j , which may or may not happen. It is a random vector whose probability to belong to cluster j will be discussed.

The space of measures of the representatives is $\mathcal{R}_s := \{\beta_c R_c + \beta_{\text{disc}} R_{\text{disc}}, R_c \in \mathcal{R}_c, R_{\text{disc}} \in \mathcal{R}_{\text{disc}}, \beta_c + \beta_{\text{disc}} = 1\}$ where

- \mathcal{R}_c is the set of the probability measures R_c for which the associated density (i.e. their Radon–Nikodým derivative with respect to the Lebesgue measure), exists, has finite support and is continuous almost everywhere in \mathbb{R}^d ,
- $\mathcal{R}_{\text{disc}}$ is the set of the probability measures of the form $R_{\text{disc}} = \sum_{k=1}^m c_k \delta_{\gamma_k}$, with δ_{γ_k} the Dirac measure at γ_k and $c_k \in [0, 1]$ such that $\sum_{k=1}^m c_k = 1$.

Then, $R_J = \beta_c R_c + \beta_{\text{disc}} \sum_{k=1}^m c_k \delta_{\gamma_k}$. We denote by f_c the probability density function (PDF) associated to R_c .

D.1 Convergence in law of the mixture samples designated by the clustering

D.1.1 Convergence in law of $a_N(X_k)$

The law of the closest sample from the mixture to the k -th data sample is similar, when N grows, to that of any representative, for example the first one.

Proposition 5. $\forall k = 1, \dots, n$, $a_N(X_k)$ converges in law to Y_1 :

$$a_N(X_k) \xrightarrow{\mathcal{L}} Y_1$$

Proof. Let $\alpha \in \mathbb{R}^d$. We denote $A(\alpha) = \{y \in \mathbb{R}^d, \forall i = 1, \dots, d, y^i \leq \alpha^i\}$. The cumulated density function (CDF) of $a_N(X_k)$ is

$$\begin{aligned} F_{a_N(X_k)}(\alpha) &= \beta_c \int_{\mathbb{R}^d} P(a_N(X_k) \in A(\alpha) \mid X = x) f_c(x) dx \\ &\quad + \beta_{\text{disc}} \sum_{r=1}^m p_r P(a_N(X_k) \in A(\alpha) \mid X = \gamma_r) . \end{aligned}$$

The proof works by showing that the CDF of $a_N(X_k)$ tends to that of Y_1 when N grows.

Limit of $\beta_{\text{disc}} \sum_{r=1}^m p_r P(a_N(X_k) \in A(\alpha) \mid X = \gamma_r)$
 If $\gamma_r \in A(\alpha)$, then $P(a_N(X_k) \in A(\alpha) \mid X = \gamma_r) \geq P(\exists i \in \{1, \dots, N\}, Y_i = \gamma_r)$.
 As a result, $P(a_N(X_k) \in A(\alpha) \mid X = \gamma_r) \xrightarrow{N \rightarrow +\infty} 1$.

Else, if $\gamma_r \notin A(\alpha)$, then $P(a_N(X_k) \in A(\alpha) \mid X = \gamma_r) \leq P(\forall i \in \{1, \dots, N\}, Y_i \neq \gamma_r)$. Consequently, $P(a_N(X_k) \in A(\alpha) \mid X = \gamma_r) \xrightarrow{N \rightarrow +\infty} 0$.

Finally, it follows that $\beta_{\text{disc}} \sum_{r=1}^m p_r P(a_N(X_k) \in A(\alpha) \mid X = \gamma_r) \xrightarrow{N \rightarrow +\infty}$

$$\beta_{\text{disc}} \sum_{r \text{ s.t. } \gamma_r \in A(\alpha)} p_r$$

Limit of $\beta_c \int_{\mathbb{R}^d} P(a_N(X_k) \in A(\alpha) \mid X = x) f_c(x) dx$

Let $x \in \mathbb{R}^d$ such that f_c is continuous at x and $x \notin \{x \in \mathbb{R}^d, \exists i \in \{1, \dots, d\}, x^i = \alpha^i\}$.

- If $f_c(x) = 0$ then $\forall N, P(a_N(X_k) \in A(\alpha) \mid X = x) f_c(x) = 0$
- Case when $x \in A(\alpha)$ and $f_c(x) > 0$. Then, $\exists(\varepsilon^1, \dots, \varepsilon^d) \in (\mathbb{R}_+^*)^d, x^k = \alpha^k - \varepsilon^k$.
By continuity, $\exists \eta \in]0, \arg \min_{1 \leq k \leq d} \varepsilon^k[, \forall x' \in \mathcal{B}(x, \eta), f_c(x') > 0$, with $\mathcal{B}(x, \eta)$ the ball of radius η and center x . This means that $P(a_N(X_k) \in A(\alpha) \mid X = x) f_c(x) \geq P(\exists i \in \{1, \dots, N\}, Y_i \in \mathcal{B}(x, \eta))$. Finally, $P(a_N(X_k) \in A(\alpha) \mid X = x) \xrightarrow{N \rightarrow +\infty} 1$.
- Case when $x \notin A(\alpha)$ and $f_c(x) > 0$. Then, $\exists \varepsilon > 0, x^k = \alpha^k + \varepsilon$. By continuity, $\exists \eta \in]0, \varepsilon[, \forall x' \in \mathcal{B}(x, \eta), f_c(x') > 0$, with $\mathcal{B}(x, \eta)$ the ball of radius η and center x . Thus, $P(a_N(X_k) \notin A(\alpha) \mid X = x) f_c(x) \leq P(\forall i \in \{1, \dots, N\}, Y_i \notin \mathcal{B}(x, \eta))$. And finally $P(a_N(X_k) \in A(\alpha) \mid X = x) \xrightarrow{N \rightarrow +\infty} 0$.

We then have, $P(a_N(X_k) \in A(\alpha) \mid X = x) f_c(x) \xrightarrow{N \rightarrow +\infty} \mathbf{1}_{A(\alpha)}(x) f_c(x)$.

The Dominated Convergence Theorem gives,

$$\beta_c \int_{\mathbb{R}^d} P(a_N(X_k) \in A(\alpha) \mid X = x) f_c(x) dx \xrightarrow{N \rightarrow +\infty} \beta_c \int_{A(\alpha)} f_c(x) dx$$

Limit of $F_{a_N(X_k)}(\alpha)$

Finally, we have,

$$F_{a_N(X_k)}(\alpha) \xrightarrow{N \rightarrow +\infty} F_Y(\alpha).$$

□

D.1.2 Convergence in law of $a_N(X_k) \mid J_{I_N(X_k)} = j$

The random vector $a_N(X_k)$, i.e., the closest mixture sample to the k -th data sample, when constrained to belong to the j -th cluster and when N grows, follows the distribution of the j -th representative R_j .

Proposition 6.

$$\forall j \in \mathcal{J}, a_N(X_k) \mid J_{I_N(X_k)} = j \xrightarrow{\mathcal{L}} Y_1 \mid J_1 = j$$

Proof. As in the previous Proposition, $\alpha = (\alpha^1, \dots, \alpha^d) \in \mathbb{R}^d$ and $A(\alpha) = \{x \in \mathbb{R}^d, \forall i = 1, \dots, d, x^i \leq \alpha^i\}$.

To shorten the notations, we write

the k -th sample point associated to the j -th cluster $\tilde{X}_{k,N}^{(j)} := X_k \mid J_{I_N(X_k)} = j$.

$$\begin{aligned}
F_{a_N(\tilde{X}_{k,N}^{(j)})}(\alpha) &= P(a_N(\tilde{X}_{k,N}^{(j)}) \in A(\alpha)) \\
&= P(a_N(X_k) \in A(\alpha) \mid J_{I_N(X_k)} = j) \\
&= \sum_{i=1}^N P(I_N(X_k) = i, Y_i \in A(\alpha) \mid J_{I_N(X_k)} = j) \\
&= NP(I_N(X_k) = 1, Y_1 \in A(\alpha) \mid J_{I_N(X_k)} = j)
\end{aligned}$$

Bayes' Theorem gives,

$$\begin{aligned}
&P(I_N(X_k) = 1, Y_1 \in A(\alpha) \mid J_{I_N(X_k)} = j) \\
&= \frac{P(J_{I_N(X_k)} = j \mid I_N(X_k) = 1, Y_1 \in A(\alpha))P(I_N(X_k) = 1, Y_1 \in A(\alpha))}{P(J_{I_N(X_k)} = j)} \\
&= \frac{P(J_1 = j \mid Y_1 \in A(\alpha))P(I_N(X_k) = 1, Y_1 \in A(\alpha))}{P(J_{I_N(X_k)} = j)} \\
&= \frac{P(Y_1 \in A(\alpha) \mid J_1 = j)P(J_1 = j)}{P(Y_1 \in A(\alpha))} \frac{P(I_N(X_k) = 1, Y_1 \in A(\alpha))}{P(J_{I_N(X_k)} = j)} \\
&= \frac{P(Y_1 \in A(\alpha) \mid J_1 = j)p_j}{P(Y_1 \in A(\alpha))} \frac{P(I_N(X_k) = 1, Y_1 \in A(\alpha))}{p_j} \\
&= \frac{P(Y_1 \in A(\alpha) \mid J_1 = j)P(I_N(X_k) = 1, Y_1 \in A(\alpha))}{P(Y_1 \in A(\alpha))}
\end{aligned}$$

Then

$$\begin{aligned}
F_{a_N(\tilde{X}_{k,N}^{(j)})}(\alpha) &= N \frac{P(Y_1 \in A(\alpha) \mid J_1 = j)P(I_N(X_k) = 1, Y_1 \in A(\alpha))}{P(Y_1 \in A(\alpha))} \\
&= \frac{P(Y_1 \in A(\alpha) \mid J_1 = j)}{P(Y_1 \in A(\alpha))} \sum_{i=1}^N P(I_N(X_k) = i, Y_i \in A(\alpha)) \\
&= P(Y_1 \in A(\alpha) \mid J_1 = j) \frac{P(a_N(X_k) \in A(\alpha))}{P(Y_1 \in A(\alpha))}
\end{aligned}$$

Proposition 5 gives $\frac{P(a_N(\tilde{X}_{k,N}^{(j)}) \in A(\alpha))}{P(Y_1 \in A(\alpha))} \xrightarrow{N \rightarrow +\infty} 1$.

As a result,

$$F_{a_N(\tilde{X}_{k,N}^{(j)})}(\alpha) \xrightarrow{N \rightarrow +\infty} P(Y_2 \in A(\alpha) \mid J_1 = j).$$

□

D.2 Wasserstein convergence to the representatives

D.2.1 Wasserstein convergence of $a_N(\tilde{X}_{k,N}^{(j)})$

The mixture sample that is both the closest to X_k and coming from R_j has a distribution that converges, in terms of Wasserstein metric, to R_j . This is a corollary of Proposition 6.

Corollary 1.

$$\mathcal{W}_p(\mu_N^j, R_j) \xrightarrow{N \rightarrow +\infty} 0,$$

where μ_N^j is the measure associated to $a_N(\tilde{X}_{k,N}^{(j)})$.

Proof. As stated in [26], convergence in p -Wasserstein distance is equivalent to convergence in law plus convergence of the p^{th} moment. As the distributions of \mathcal{R} have bounded supports, $X \xrightarrow{\mathcal{L}} Y \implies E(\|X\|^p) = E(\|Y\|^p)$. \square

D.2.2 Wasserstein convergence of $(a_N(\tilde{X}_{k,N}^{(j)}))_{k=1}^n$

The above Wasserstein convergence to the j -th representative for a given data sample X_k also works on the average of the X_k 's as their number n grows.

Proposition 7.

$$\lim_{n, N \rightarrow +\infty} \mathbb{E}(\mathcal{W}_p(\mu_{n,N}^j, R_j)) = 0,$$

where $\mu_{n,N}^j$ is the empirical measure associated to $(a_N(\tilde{X}_{k,N}^{(j)}))_{k=1}^n$.

Proof. By the triangle inequality applied to the $\mathcal{W}_p(\cdot, \cdot)$ metric,

$$\mathbb{E}(\mathcal{W}_p(\mu_{n,N}^j, R_j)) \leq \mathbb{E}(\mathcal{W}_p(\mu_{n,N}^j, \mu_N^j)) + \mathbb{E}(\mathcal{W}_p(\mu_N^j, R_j)).$$

As the distributions of \mathcal{R}_s have a bounded support, then for all $q \in \mathbb{N}$, $\exists M_1, \forall N \in \mathbb{N}, \int_{\mathbb{X}} |x|^q \mu_N^j(dx) \leq M_1$.

Then, as shown in [7],

$$\exists M_2, \forall N \in \mathbb{N}, \mathbb{E}(\mathcal{W}_p(\mu_{n,N}^j, \mu_N^j)) \leq M_2 G(n)$$

where $G(n) \xrightarrow{n \rightarrow +\infty} 0$.

Let $\varepsilon > 0$,

$$\exists n_0, \forall n > n_0, \forall N, \mathbb{E}(\mathcal{W}_p(\mu_{n,N}^j, \mu_N^j)) < \frac{\varepsilon}{2},$$

and Corollary 1 gives

$$\exists N_0, \forall N > N_0, \mathbb{E}(\mathcal{W}_p(\mu_N^j, R_j)) < \frac{\varepsilon}{2}.$$

Finally,

$$\forall n, N > \max(n_0, N_0), \mathbb{E}(\mathcal{W}_p(\mu_{n,N}^j, R_j)) < \varepsilon.$$

\square

D.2.3 Wasserstein convergence of $C_j^*(R, J, n, N)$ to R_j

The j -th cluster produced by the *FindC* algorithm, $C_j^*(R, J, n, N)$, can be seen as the i.i.d. sample $(\tilde{X}_{k,N}^{(j)})_{k=1}^{n_j}$, with $\sum_{j=1}^{\ell} n_j = n$. We have $n_j \rightarrow +\infty$ when $n \rightarrow +\infty$, provided $p_j > 0$.

We denote $\nu_{n_j,N}^j$ the empirical measure associated to $(\tilde{X}_{k,N}^{(j)})_{k=1}^{n_j}$. The triangle inequality implies that

$$\mathbb{E}(\mathcal{W}_p(\nu_{n_j,N}^j, R_j)) \leq \mathbb{E}(\mathcal{W}_p(\nu_{n_j,N}^j, \mu_{n_j,N}^j)) + \mathbb{E}(\mathcal{W}_p(\mu_{n_j,N}^j, R_j)) .$$

Furthermore,

$$\begin{aligned} \mathbb{E}(\mathcal{W}_p(\nu_{n_j,N}^j, \mu_{n_j,N}^j)) &\leq \mathbb{E}\left(\frac{1}{n_j} \sum_{k=1}^{n_j} \|\tilde{X}_{k,N}^{(j)} - a_N(\tilde{X}_{k,N}^{(j)})\|^p\right) \\ &\leq \mathbb{E}(\|\tilde{X}_{1,N}^{(j)} - a_N(\tilde{X}_{1,N}^{(j)})\|^p) \\ &\leq \mathbb{E}(\|X_1 - a_N(X_1)\|^p | J_{I_N}(X_1) = j) \end{aligned}$$

The law of total expectation gives

$$\mathbb{E}(\|X_1 - a_N(X_1)\|^p) = \sum_{j=1}^{\ell} p_j \mathbb{E}(\|X_1 - a_N(X_1)\|^p | J_{I_N}(X_1) = j) .$$

Since $a_N(X_k)$ is the closest sample in $\{Y_1, \dots, Y_N\}$ to X_k , we have

$$\begin{aligned} \mathbb{E}(\|X_1 - a_N(X_1)\|^p) &= \mathbb{E}\left(\frac{1}{N} \sum_{k=1}^N \|X_k - a_N(X_k)\|^p\right) \\ &\leq \mathbb{E}(\mathcal{W}_p((X_k)_{k=1}^N, (Y_i)_{i=1}^N)) \xrightarrow{N \rightarrow +\infty} 0 \end{aligned}$$

The last two relations give,

$$\forall j \in \mathcal{J}, \mathbb{E}(\|X_1 - a_N(X_1)\|^p | J_{I_N}(X_1) = j) \xrightarrow{N \rightarrow +\infty} 0$$

Therefore,

$$\begin{cases} \lim_{n_j, N \rightarrow +\infty} \mathbb{E}(\mathcal{W}_p(\nu_{n_j,N}^j, \mu_{n_j,N}^j)) = 0 , \\ \text{and, by Proposition 7, } \lim_{n_j, N \rightarrow +\infty} \mathbb{E}(\mathcal{W}_p(\nu_{n_j,N}^j, R_j)) = 0 . \end{cases}$$

D.3 Convergence of the expected quantization error

We have

$$\begin{aligned} \mathcal{E}_p(\mathbf{C}^*(R, J, n, N)) &= \left(\sum_{j \in \mathcal{J}} p_j w_p(C_j^*(R, J, n, N))^p \right)^{1/p} \\ &\leq \sum_{j \in \mathcal{J}} p_j w_p(C_j^*(R, J, n, N)) \end{aligned}$$

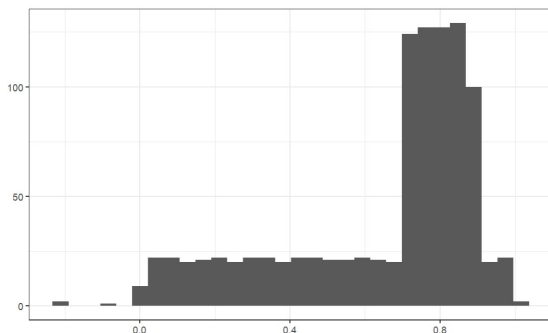


Figure 16: Distribution of the sample S_{EM} .

By definition of the local clustering error, for $j \in \mathcal{J}$, $w_p(C_j^*(R, J, n, N)) \leq \mathcal{W}_p(C_j^*(R, J, n, N), R_j)$. As just seen in Section D.2.3,

$$\lim_{n_j, N \rightarrow +\infty} \mathbb{E} \left(\mathcal{W}_p(\nu_{n_j, N}^j, R_j) \right) = \lim_{n, N \rightarrow +\infty} \mathbb{E} \left(\mathcal{W}_p(C_j^*(R, J, n, N), R_j) \right) = 0 .$$

Then,

$$\lim_{n, N \rightarrow +\infty} \mathbb{E} \left(w_p(C_j^*(R, J, n, N)) \right) = 0 ,$$

and finally,

$$\lim_{n, N \rightarrow +\infty} \mathbb{E} \left(\mathcal{E}_p(\mathbf{C}^*(R, J, n, N)) \right) = 0 .$$

E Merging the split clusters

The $\ell + \ell_{\text{bin}}$ clusters that were created by splitting are merged back into ℓ clusters by trying all possible combinations and keeping the best one in terms of quantization error. Algorithm 5 details the procedure. The set of all the perturbations tried, $G(\mathbf{C})$, is built in the algorithm and is the union of all the $\hat{\mathbf{C}}$. Since the initial clustering is one of the combinations tried, the result of *Perturb (split and merge)* is guaranteed not to be worse than the initial clustering, as stated in Proposition 4.

Algorithm 5 *merge procedure*

Input: Sample $(x_i)_{i=1}^n$, a partition $\hat{C} = (\hat{C}_1, \dots, \hat{C}_{\ell+\ell_{\text{bin}}})$

```
 $C^* \leftarrow \emptyset$   
 $\mathcal{E}^* \leftarrow \infty$   
 $\mathcal{P} = \{ \mathcal{P} : \text{partition of } 1, \dots, \ell + \ell_{\text{bin}} \text{ in } \ell \text{ groups} \}$   
for  $\mathcal{P} \in \mathcal{P}$  do  
   $(G_1, \dots, G_\ell) \leftarrow \mathcal{P}$   
  for  $j \in 1 : \ell$  do  
     $\hat{C}_j = \bigcup_{k \in G_j} \hat{C}_k$   
  end for  
   $\hat{C} \leftarrow (\hat{C}_1, \dots, \hat{C}_\ell)$   
   $\mathcal{E} \leftarrow \mathcal{E}_p(\hat{C})$   
  if  $\mathcal{E} < \mathcal{E}^*$  then  
     $C^* = (C_1^*, \dots, C_\ell^*) \leftarrow \hat{C}$   
     $\mathcal{E}^* \leftarrow \mathcal{E}$   
  end if  
end for
```

Output: $C^* = (C_1^*, \dots, C_\ell^*)$

F An implementation of the Augmented Quantization algorithm

The implemented version of the Augmented Quantization algorithm is detailed in Algorithm 6 hereafter. It is based on a repetition of epochs during where the perturbation intensity (controlled by the relative size of the cluster bins, p_{bin}). An epoch is made of cycles of the *FindC*, *Perturb* and *FindR* steps until convergence of the representatives or a maximum number of cycles. Between epochs, p_{bin} is decreased. An empirical tuning of the algorithm's parameters led to the following values: p_{bin} decreases according to $\text{list-}p_{\text{bin}} = [0.4, 0.2, 0.1]$; the maximal number of (*FindC*, *Perturb*, *FindR*) iterations at a constant p_{bin} is $t_{\text{max}} = 10$ and the convergence threshold in terms of distance between successive representatives is $\text{MinDistance} = 10^{-2}$.

Algorithm 6 Detailed Augmented quantization algorithm

Input: a sample $(x_i)_{i=1}^n$, $\mathbf{R} = (R_1, \dots, R_\ell) \in \mathcal{R}^\ell$, $\text{list_}p_{\text{bin}}$, it_{max} , minDistance

J random variable with $P(J = j) = \frac{1}{\ell}$
 $(\mathbf{R}^*, \mathbf{C}^*, \mathcal{E}^*) \leftarrow (\emptyset, \emptyset, +\infty)$
for $p_{\text{bin}} \in \text{list_}p_{\text{bin}}$ **do**
 $\text{dist} \leftarrow +\infty$
 $\text{it} \leftarrow 1$
 while $\text{dist} > \text{minDistance}$ AND $\text{it} \leq \text{it}_{\text{max}}$ **do**
 $\mathbf{R}^{\text{old}} \leftarrow \mathbf{R}$
 $\mathbf{C} \leftarrow \text{FindC}(\mathbf{R}, J)$
 $\mathbf{C} \leftarrow \text{Perturb}(\mathbf{C}), p_{\text{bin}}$
 $\mathbf{R} \leftarrow \text{FindR}(\mathbf{C})$
 J r.v. with $P(J = j) = \frac{\text{card}(\mathcal{C}_j)}{n}$, $j \in \mathcal{J}$
 if $\mathcal{E}_p(\mathbf{C}, \mathbf{R}) < \mathcal{E}^*$ **then** $\mathcal{E}^* \leftarrow \mathcal{E}$, $\mathbf{C}^* \leftarrow \mathbf{C}$, $\mathbf{R}^* \leftarrow \mathbf{R}$, $J^* \leftarrow J$
 end if
 $\text{it} \leftarrow \text{it} + 1$
 $\text{dist} \leftarrow \text{distance}(\mathbf{R}^{\text{old}}, \mathbf{R})$
 end while
end for

Output: $R_{J^*}^*$

G Evolution of the quantization error

The evolution of the quantization errors in time for the uniform, the Gaussian and the hybrid test cases is depicted in Figure 17. Each sample test is represented with a different color. The plots highlight that 10 iterations are typically adequate for reaching the optimal quantization error. The most substantial reduction in error occurs during the initial iteration. Occasional minor increases in error arise during the *FindC* step, whose convergence guarantees are only asymptotic (Proposition 3).

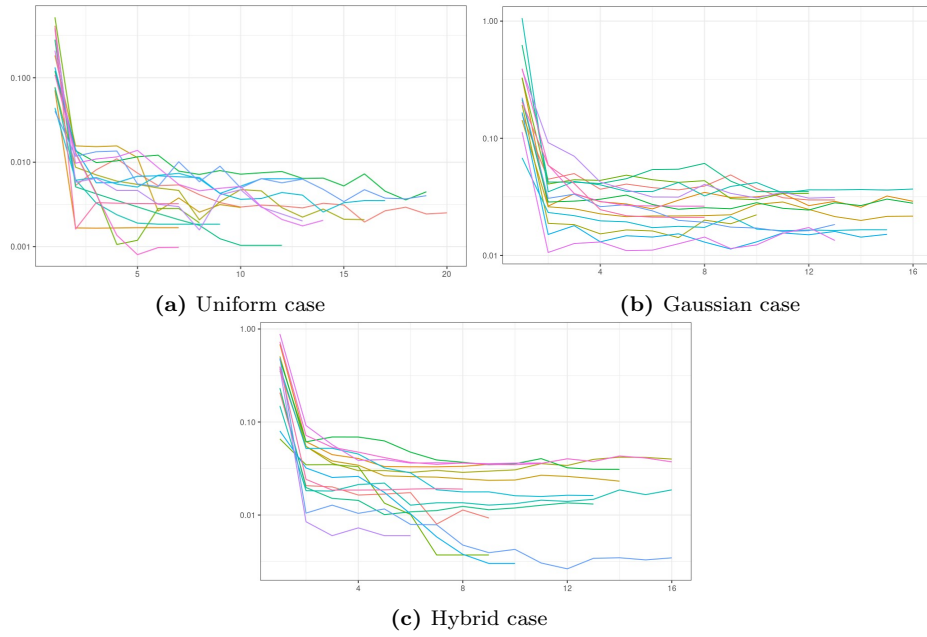


Figure 17: Evolution of the quantization error throughout the iterations over 15 experiment repetitions.

H Flooding prototype maps

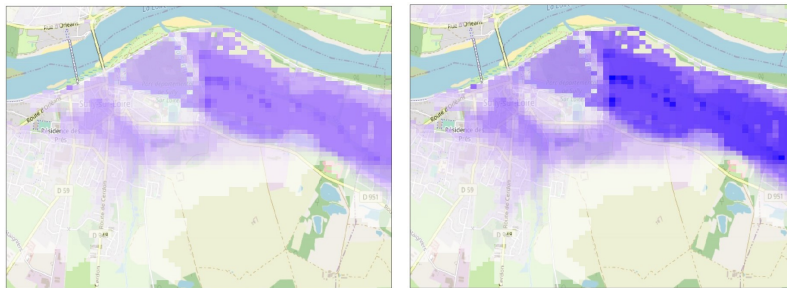


(a) $P = 9.9 \times 10^{-1}$



(b) $P = 3.5 \times 10^{-3}$

(c) $P = 1.5 \times 10^{-3}$



(d) $P = 8.9 \times 10^{-4}$

(e) $P = 5.8 \times 10^{-4}$

Figure 18: The 5 flooding prototype maps in the Loire case study.